


Article

Suitable Land-Use and Land-Cover Allocation Scenarios to Minimize Sediment and Nutrient Loads into Kwan Phayao, Upper Ing Watershed, Thailand

Jiraporn Kulsoontornrat ^{1,2} and Suwit Ongsomwang ^{1,*} 

¹ Institute of Science, School of Geoinformatics, Suranaree University of Technology, Nakhon Ratchasima 30000, Thailand; j.kulsoontornrat@gmail.com

² Department of Geographic Information Science, School of Information and Communication Technology, University of Phayao, Muang Phayao 56000, Thailand

* Correspondence: suwit@sut.ac.th; Tel.: +66-8-9895-8149

Abstract: Human activity and land-use changes have affected the water quality of Kwan Phayao, Upper Ing watershed, due to the associated high sediment load and eutrophication. This study aims to identify suitable LULC allocation scenarios for minimizing sediment and nutrient export into the lake. For this purpose, the LULC status and change were first assessed, based on classified LULC data in 2009 and 2019 from Landsat images, using the SVM algorithm. Later, the land requirements of three scenarios between 2020 and 2029 were estimated, based on their characteristics, and applied to predict LULC change using the CLUE-S model. Then, actual LULC data in 2019 and predicted LULC data under three scenarios between 2020 and 2029 were used to estimate sediment and nutrient export using the SDR and NDR models. Finally, the ecosystem service change index identified a suitable LULC allocation for minimizing sediment or/and nutrient export. According to the results, LULC status and change indicated perennial trees and orchards, para rubber, and rangeland increased, while forest land and paddy fields decreased. The land requirements of the three scenarios provided reasonable results, as expected, particularly Scenario II, which adopts linear programming to calculate the land requirements for maximizing ecosystem service values. For sediment and nutrient export estimation under the predicted LULC for the three scenarios, Scenario II led to the lowest yield of sediment and nutrient exports, and provided the lowest average ESCI value among the three scenarios. Thus, the LULC allocation under Scenario II was chosen as suitable for minimizing sediment or/and nutrient export into Kwan Phayao. These results can serve as crucial information to minimize sediment and nutrient loads for land-use planners, land managers, and decision makers.

Keywords: land-use and land-cover allocation; sediment and nutrient export; CLUE-S model; InVEST model; Kwan Phayao; Upper Ing watershed



Citation: Kulsoontornrat, J.; Ongsomwang, S. Suitable Land-Use and Land-Cover Allocation Scenarios to Minimize Sediment and Nutrient Loads into Kwan Phayao, Upper Ing Watershed, Thailand. *Appl. Sci.* **2021**, *11*, 10430. <https://doi.org/10.3390/app112110430>

Academic Editors: Huaguo Huang and Lin Sun

Received: 14 October 2021

Accepted: 3 November 2021

Published: 5 November 2021

Publisher's Note: MDPI stays neutral with regard to jurisdictional claims in published maps and institutional affiliations.



Copyright: © 2021 by the authors. Licensee MDPI, Basel, Switzerland. This article is an open access article distributed under the terms and conditions of the Creative Commons Attribution (CC BY) license (<https://creativecommons.org/licenses/by/4.0/>).

1. Introduction

Freshwater ecosystems are considered as one of the essential natural resources for living organisms. The rate of deterioration of the water quality of freshwater resources, such as lakes, ponds, and rivers, has become a global problem [1]. Lakes are vital components of our planet's hydrological cycle, providing significant social and ecological functions while storing water and supporting aquatic biodiversity [2]; however, they are often the final recipients of nutrients discharged from adjacent uplands and wetlands. The management of a lake means managing its watershed—which are often mismanaged and challenged natural resources. Some problems originate in the lake itself, but most problems originate from activities occurring on the surrounding land [3]. Several studies have shown that land uses play essential roles determining the water quality of lakes. In particular, urban, built-up, and cultivated areas significantly influence the water quality when within the

lake basin [4,5]. Furthermore, land-use and land-cover changes are significant drivers of the accelerated eutrophication of surface waters, due to soil loss and nutrient loading into water bodies. Agricultural soil losses also have an impact on sediment deposition [6].

Meanwhile, land-use changes lead to changes in ecosystem services (ESs). The impacts of various land uses on ESs occur in three ways: major ESs are generated under different land-use practices, land-use patterns have a significant impact on ESs, and differing intensities of land use may have different impacts on the generation of ESs [7]. Ecosystem services are the utilities that people obtain from ecosystems. These include provisioning, regulating, cultural, and supporting services [8,9]. Thus, the assessment of ecosystem services and their relationship to human well-being requires an integrated approach. The modeling of land-use changes provides effective methods to estimate the impact on the environment and ecosystem services [10–12], and ecosystem services models such as InVEST (Integrated Valuation of Ecosystem Services and Trade-offs) have been used to assess and model ecosystem services quantitatively, as well as to analyze and map ecosystem services through GIS-based spatially explicit modeling tools. Additionally, InVEST can be used to estimate the monetary value of ecosystem services [13]. For example, Srichaichana et al. [14] have applied toolsets for multiple ecosystem service evaluations—namely water yield and sediment delivery ratio models—to estimate water yield and sediment retention ecosystem services in the Klong U-Tapao watershed, Songkhla Province, Thailand, for the mitigation of flooding by reducing runoff and the prevention of soil erosion by increasing sediment retention in the basin.

Kwan Phayao or Phayao lake is the largest freshwater lake in the Northern region and the fourth largest in Thailand, and has been classified in the list of wetlands of international importance. This lake is an essential source of food security and species diversity conservation. About 36 species of aquatic plants are found in the lake [15], and 44 species of fish have been identified [16]. Furthermore, Kwan Phayao provides various ecosystem services, including water supply for household consumption, agriculture, and recreation.

Kwan Phayao is situated in the Upper Ing watershed, where the Nam Mae Ing River flows from Nong Leng Sai, located at the northern end and pouring into the lake, while Nam Mae Tum River, at the southern end, also inflows to the lake. Primary cultivation practices in the watershed include paddy fields, field crops, and perennial trees and orchards. The extent of the Phayao Municipality has rapidly expanded due to an increase in population. These activities have created many environmental problems, such as non-point source (NPS) pollution and soil erosion. Additionally, changes in land uses, such as urban and agriculture transitions, have affected the water quality of the lake. This effect is due to the excessive amounts of nutrients (e.g., nitrogen and phosphorus) originating from agriculture practices and human activities. The nutrient flow into the lake causes plankton blooms or eutrophication, as well as the spread of toxic algal diversity [17], chlorophytic phytoplankton [18], and water hyacinths [19]. Furthermore, the lake is becoming shallower due to the high sediment load arising from soil erosion [20].

Consequently, in this paper, suitable LULC allocation at the Upper Ing watershed for reducing nutrient and sediment loads into Kwan Phayao under different scenarios is examined by integrating remote sensing to classify LULC data, a land-use change model (CLUE-S model) to predict LULC data, and an ecosystem services modeler (the SDR and NDR models of the InVEST software) to estimate sediment and nutrient exports. Our specific research objectives were: (1) to classify LULC data in 2009 and 2019; (2) to estimate the land requirements and predict the LULC of three scenarios between 2020 and 2029; (3) to estimate sediment and nutrient export of actual LULC in 2019 and predicted LULC of three scenarios between 2020 and 2029, and (4) to identify suitable LULC allocation to minimize sediment or/and nutrient export.

2. Study Area

The Upper Ing watershed is a part of the Mekong basin, where the Ing River is the main stream, which flows northward into the Mekong River at Chiang Kong district,

Chiang Rai province. The watershed area is about 891.35 sq. km, and it covers two whole districts (Mueang Phayao and Mae Chai) of the Phayao province and some parts of two districts (Phan and Phadad) of the Chiang Rai province. The watershed is located between 19°01'21" N to 19°32'53" N and 99°41'24" E to 99°57'32" E (see Figure 1).

In this watershed, there are two crucial wetland areas: Kwan Phayao and Nong Leng Sai. The highland and mountains are on the west side, while the areas between the floodplain and highland are undulating and rolling plains. The lowest area in the study area is Kwan Phayao, which collects and stores water, sediments, and nutrients from upstream in the northwest and west parts of the watershed.

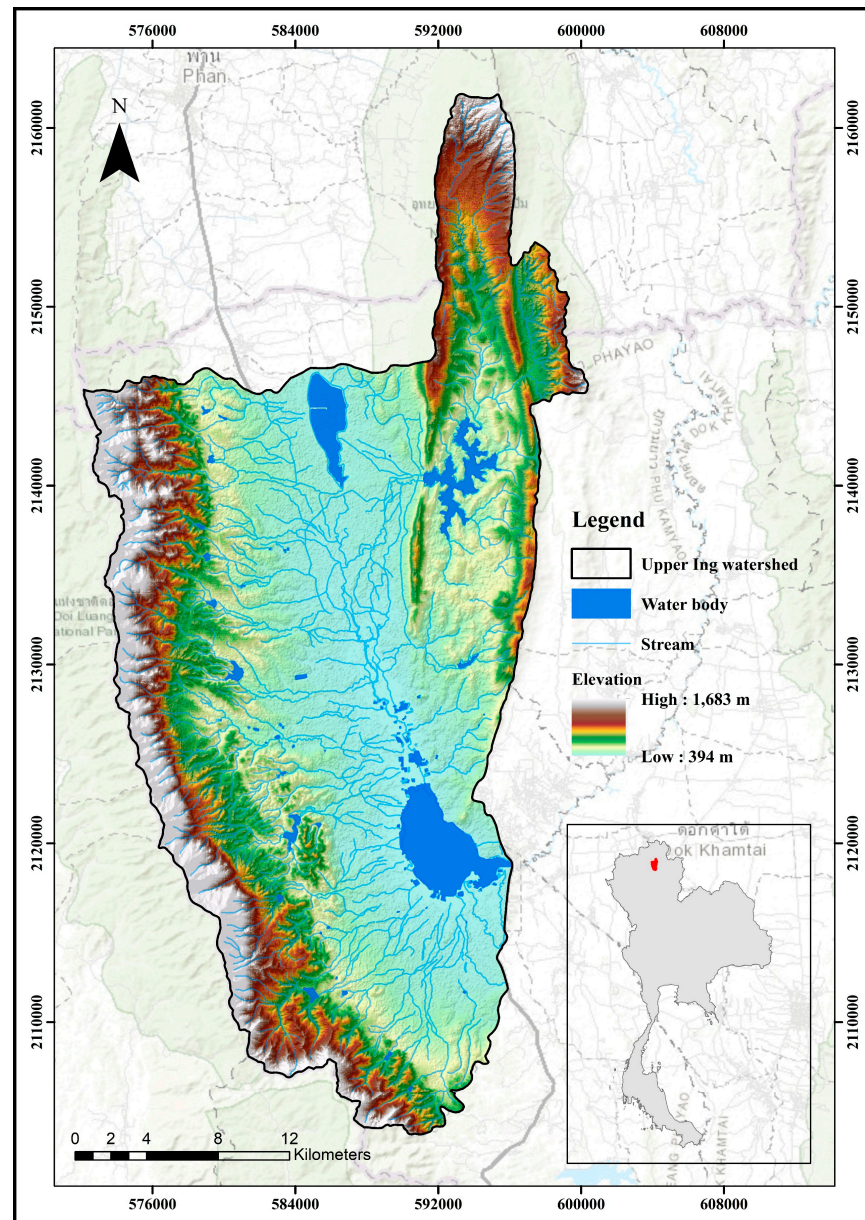


Figure 1. Location map and topographic feature of the Upper Ing watershed, Mekong basin.

The problems related to Kwan Phayao have recently been reported by the Department of Fisheries and Royal Irrigation Department, as summarized in Table 1. The Ministry of Agriculture and Cooperative has spent about 4 million USD to increase water storage by sediment dredging, aquatic plant weeding, and flap-gate-weir building [20].

Table 1. The existing problems related to Kwan Phayao.

State of Problems	
1.	Water flowing into the lake is less than 33.84 million cubic meters.
2.	Total sediment is 134,459 tons per year (95,200 cubic meters per year).
2.1.	Sediment from water hyacinth and aquatic weed are 103,430 tons per year.
2.2.	Sediment from erosion is 31,029 tons per year.
3.	The expansion of the weed covers 4.414 square kilometers of the water surface (or about 21.6% of the water surface).
4.	Water demand for irrigation is 15 million cubic meters per year.

Source: [20,21].

3. Materials and Methods

The research methodology consisted of data collection and preparation, in five significant components (Figure 2).

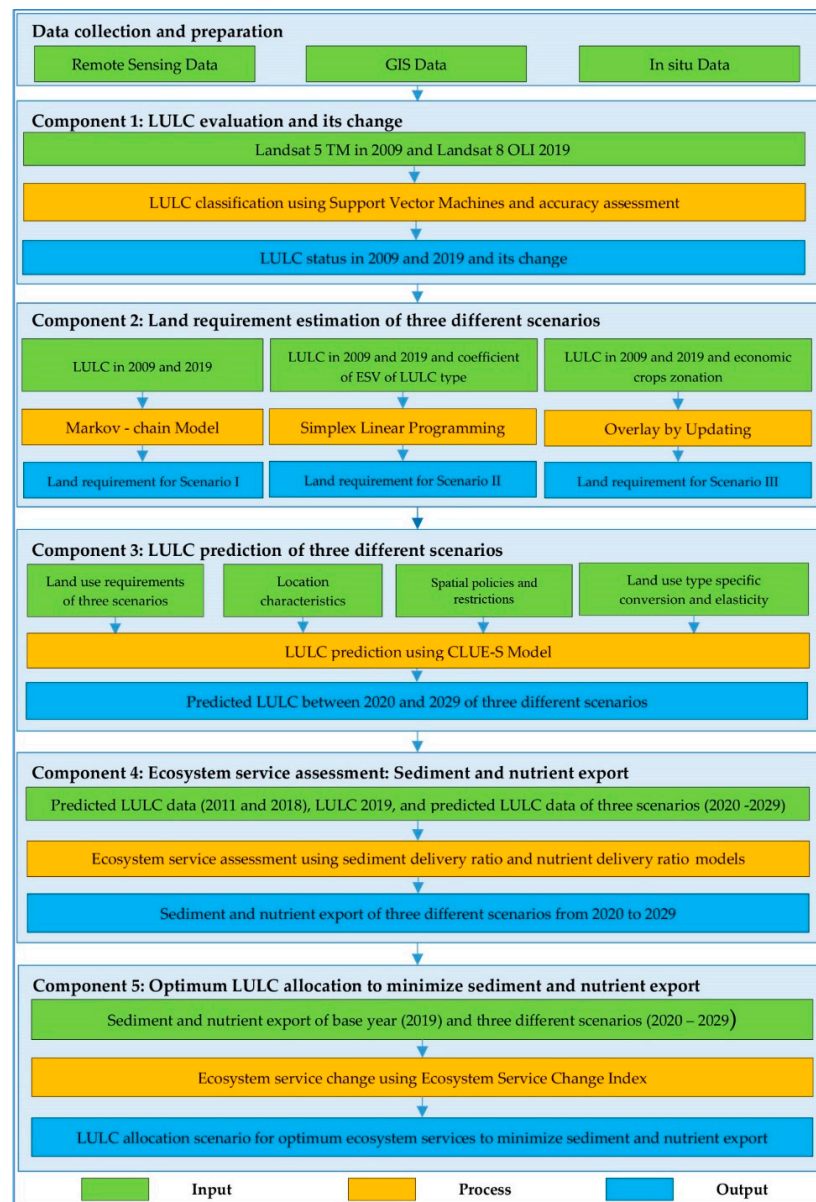


Figure 2. Workflow of research methodology.

3.1. Data Collection and Preparation

The required input data for data analysis included GIS, remote sensing, and relevant data, as summarized in Table 2.

Table 2. List of data collection for data analysis in this study.

Data	Data Collection	Source
GIS	Land-use data in 2009	LDD
	Land-use data in 2015	LDD
	Watershed boundary	DEQP
	SRTM DEM	USGS
	Soil drainage	LDD
	Stream network	DEQP
	Waterbody	DEQP
	Villages	LDD
	Road network	LDD
	Fault line	DMR
	Income per capita at subdistrict level	NSO
	Population density at subdistrict level	DOPA
	Soil series map	[22]
	Geology unit map	[22]
	Agri-Map	[23]
Remote Sensing	Landsat 5 TM, Date 27 February 2009	USGS
	Landsat 8 OLI, Date 23 February 2019	USGS
	Google Image 2009 and 2010	Google Earth
Secondary data	Annual and monthly rainfall between 2011 and 2019	TMD
	C-factor and P-factor	[22]
	Predicted rainfall between 2020 and 2029	[24]
	Nitrogen/Phosphorus loading	[25]
	Nitrogen retention coefficients	[25]
	Phosphorus retention coefficients	[25]
	Total suspended solids/Total phosphorus/Total nitrogen between 2011 and 2018	PCD
Annual surface runoff between 2011 and 2018	RID	
Tools and models	EnMap-Box software	EnMAP
	Linear Programming with Simplex method	What's Best in Excel
	CLUE-S model	[26]
	SDR and NDR models of InVEST software	NatCap
	Ecosystem Services Change Index (ESCI)	[27]

Note: DEQP: Department of Environmental Quality Promotion; DMR: Department of Mineral Resources; DOPA: Department of Provincial Administration; EnMAP: Environmental Mapping and Analysis Program; LDD: Land Development Department; MRC: Mekong River Commission; NatCap: Natural Capital Project; NCAR: National Center for Atmospheric Research; NSO: National Statistical Office of Thailand; PCD: Pollution Control Department; RID: Royal Irrigation Department; TMD: Thai Meteorological Department; USGS: United States Geological Survey.

3.2. LULC Classification and Change Detection

We downloaded Landsat 5 TM data in 2009 and Landsat OLI data in 2019 from the USGS website (www.earthexplorer.usgs.gov; accessed date 1 May 2019), which were applied to classify LULC data by conducting supervised classification using the support vector machine (SVM) algorithm of the EnMap-Box software. Two training areas for ten LULC types were separately prepared in order to define an optimal hyperplane for LULC classification using SVM. The scaled reflectance data of Landsat data (visible, NIR, and SWIR bands) and additional bands, Normalized Difference Vegetation Index (NDVI) [28], Normalized Difference Moisture Index (NDMI) [29], Soil-Adjusted Vegetation Index (SAVI) [30], Modified Normalized Difference Wetness Index (MNDWI) [31], and DEM were applied to classify the LULC map in 2009 and 2019. The optimized model parameters were provided by a grid search: namely, Gaussian radial basis function kernel,

which required the variables gamma (γ), which defines the width of the Gaussian, and the regularization parameter (C), which controls the trade-off between the maximization of the margin between the training data vectors and the decision boundary plus the penalization of training errors [32].

The standard land-use classification of the LDD—including (1) urban and built-up area, (2) paddy field, (3) field crop, (4) para rubber, (5) perennial trees and orchards, (6) forest land, (7) water body, (8) rangeland, (9) wetland, and (10) miscellaneous land—was modified to classify the LULC type and to extract the coefficient value of each LULC type for ecosystem service value (ESV) evaluation (Table 3).

After classification, the LULC maps in 2009 and 2019 were assessed, in terms of thematic accuracy, based on reference information from very high spatial resolution images from Google Earth in 2009/2010 and a field survey in 2020, respectively. The number of sample points used for the accuracy assessment was 788, based on multinomial distribution, and sample points were allocated using the stratified random sampling technique suggested by [33]. Final LULC maps in 2009 and 2019 were further used to detect LULC change, using a post-classification comparison algorithm to describe from-to change information between 2009 and 2019, as suggested by [34,35].

Table 3. Description of LULC classification system.

No	LULC Classification for SVM	LULC Classification for ESV ¹	Coefficient Values (USD/ha/Year) ¹	Land-Use Classification ²
1	Urban and built-up area (UR)	Construction land	12.7	Urban and built-up area
2	Paddy field (PD)	Cultivated land	1032.3	Paddy field
3	Field crop (FC)	Cultivated land	1032.3	Cassava, sugarcane, and maize
4	Para rubber (RB)	Forest land	1949.0	Rubber plantation
5	Perennial trees and orchards (PO)	Forest land	1949.0	Mixed perennial trees and orchards which exclude para rubber
6	Forest land (FO)	Forest land	1949.0	Natural forest and man-made forest
7	Water body (WB)	Water body	6873.7	River, canal, natural water resource, reservoir, pond, irrigation canal
8	Rangeland (RL)	Rangeland	808.6	Scrub, grass, and pasture
9	Wetland (WL)	Wetland	9368.7	Marsh and swamp
10	Miscellaneous land (ML)	Unused land	96.3	Bush fallow, mine, laterite pit, soil pit, garbage dump, landfill, rock outcrop

Note: ¹ [36], ² [23].

3.3. Land Demand Estimation of Three Different Scenarios

The land requirements under three different scenarios for LULC prediction between 2020 and 2029 were estimated based on their characteristics, as follows:

(1) Scenario I (Trend of LULC evolution): The land requirements were calculated based on the annual change rate of LULC between 2009 and 2019 from the transition area matrix using the Markov Chain model.

(2) Scenario II (Maximization of ecosystem service values): The land requirements were calculated based on LULC allocation for maximizing ESV using Linear Programming (LP) with the Simplex method. The objective function and constraints were solved to maximize ecosystem service values using Equation (1), based on the coefficient values for the ESs of each LULC type (Table 3).

$$Z_{max} = [12.7(X_1) + 1032.3(X_2) + 1032.3(X_3) + 1949.0(X_4) + 1949.0(X_5) + 1949.0(X_6) + 6873.7(X_7) + 808.6(X_8) + 9368.7(X_9) + 96.3(X_{10})], \quad (1)$$

where Z_{max} is the objective function of scenario II for ESV maximization, X_1 is the urban and built-up area (UR), X_2 is paddy field (PD), X_3 is field crop (FC), X_4 is para rubber (RP),

X_5 is perennial trees and orchards (PO), X_6 is forest land (FO), X_7 is water body (WB), X_8 is rangeland (RL), X_9 is wetland (WL), and X_{10} is miscellaneous land.

(3) Scenario III (Economic crop zonation): The suitable zonation of four economic crops (paddy field, field crop, para rubber, and perennial trees and orchards) of LDD in 2018 was updated using the existing LULC data for 2019 in order to estimate the land requirements.

3.4. LULC Prediction of Three Different Scenarios

LULC prediction between 2020 and 2029 for the three scenarios was conducted using the CLUE-S model. In practice, the selected driving factors of LULC change (soil drainage, distance to stream, distance to water body, distance to village, slope, distance to road, distance to fault line, annual rainfall, elevation, income per capita, and population density at subdistrict level), as suggested by [37], were first examined in terms of their multicollinearity, using the variance inflation factor (VIF) to prevent the correlation of driving factors. As a general rule of thumb, the VIF value should not exceed 10 [38,39]. Then, binary logistic regression analysis was performed to identify the significant driving factors for specific LULC type allocations (Equation (2)):

$$\text{Log}\left(\frac{P_i}{1 - P_i}\right) = \beta_0 + \beta_1 X_{1,i} + \beta_2 X_{2,i} \dots + \beta_n X_{n,i}, \quad (2)$$

where P_i is the probability of a grid cell for the considered land-use type at location i , and the X values are the location factors. The coefficients (β) are estimated through logistic regression, using the actual land-use pattern as the dependent variable [40].

After that, two sets of local parameters for LULC prediction using the CLUE-S model—namely, the conversion matrix and elasticity of LULC change—were prepared. These parameters were considered and set up based on the transition probability matrix of LULC data between 2009 and 2019. The conversion matrix, which indicates the LULC change opportunity among LULC types, is assigned a value of 1 when it is allowed, or 0 when it is not allowed. Meanwhile, the elasticity values imply the probability of land-use change, which ranges from 0 (easily converted) to 1 (irreversible change), and are set up according to the transition probability matrix in the past period [26,41]. In this study, elasticity values were assigned according to the transition probability matrix of LULC change between 2019 and 2029 by the Markov Chain model, as suggested by Ongsomwang and Iamchuen [42].

Finally, the conversion matrix, the elasticity of LULC change, and land requirements under different scenarios were combined to predict LULC change data between 2020 and 2029, according to the driving factors of LULC change for specific LULC type location preference.

3.5. Ecosystem Services Assessment: Sediment and Nutrient Export

The base year LULC in 2019 and the predicted LULC between 2020 and 2029 of three scenarios, as primary input data, were used to estimate sediment and nutrient exports through the SDR and NDR models in the InVEST software suite.

3.5.1. Sediment Export Estimation

The sediment export is the amount of sediment eroded in the watershed from overland sources and delivered to the stream. In principle, the SDR model is first applied to calculate the amount of annual soil loss, using the Revised Universal Soil Loss Equation (RUSLE) of [43]:

$$A_i = R_i \cdot K_i \cdot LS_i \cdot C_i \cdot P_i, \quad (3)$$

where A_i is the annual soil erosion ($\text{ton} \cdot \text{ha}^{-1} \cdot \text{yr}^{-1}$), R_i is the rainfall erosivity ($\text{MJ} \cdot \text{mm} \cdot \text{ha}^{-1} \cdot \text{h}^{-1} \cdot \text{y}^{-1}$), K_i is the soil erodibility ($\text{ton} \cdot \text{ha} \cdot \text{hr} \cdot (\text{MJ} \cdot \text{ha} \cdot \text{mm})^{-1}$), LS_i is the slope length-gradient factor, C_i is the crop-management factor, and P_i is a support practice factor for erosion control.

The required input data for annual soil erosion are summarized below.

(1) The Rainfall erosivity factor (R) was calculated based on monthly rainfall data, as suggested by [44], as:

$$R = \sum_{i=1}^{12} 1.735 \times 10^{(1.5 \log_{10}(\frac{P_i^2}{P}) - 0.08188)}, \quad (4)$$

where R is the rainfall erosivity factor ($\text{MJ mm ha}^{-1} \text{ h}^{-1} \text{ y}^{-1}$), P_i is the monthly rainfall (mm), and P is the annual rainfall (mm).

We collected monthly rainfall data between 2011 and 2019 from TMD for model calibration and validation and actual sediment export estimation in 2019. Simulated rainfall data between 2020 and 2029 were collected from the National Center for Atmospheric Research (NCAR), for sediment export estimation under three scenarios.

(2) The Soil erodibility (K) erodibility was extracted from the soil series data of LDD, whereas its value under the slope complex in the soil map was extracted from the geology unit (Table A1 in Appendix A).

(3) The Slope length gradient factor (LS) was calculated from the DEM with a method developed by [45], as follows:

$$LS_i = S_i \frac{(A_{i-in} + D^2)^{m+1} - A_{i-in}^{m+1}}{D^{m+2} \cdot x_i^m \cdot (22.13)^m}, \quad (5)$$

where S_i is the slope factor for a grid cell, calculated as a function of the slope radians θ ($S = 10.8 \cdot \sin\theta + 0.03$ where $\theta < 9\%$, or $S = 16.8 \cdot \sin\theta - 0.50$, where $\theta \geq 9\%$); A_{i-in} is the contributing area (m^2) at the inlet of a grid cell, which is computed using the d -infinity flow direction method; D is the grid cell linear dimension; $x_i = |\sin \alpha_i| + |\cos \alpha_i|$, where α_i is the aspect direction for grid cell i , and m is the RUSLE length exponent factor.

(4) The crop management (C) and support practice (P) factors for erosion control, according to LULC type, are summarized in Table A2 in Appendix A.

Then, the model calculates the sediment delivery ratio using a connectivity index (IC), threshold flow accumulation, and maximum SDR to indicate sediment retention. The SDR value was calculated, as suggested by [46], as:

$$SDR_i = \frac{SDR_{max}}{1 + \exp\left(\frac{IC_0 - IC_i}{k}\right)}, \quad (6)$$

where SDR_{max} is the maximum theoretical SDR, set to an average value of 0.8 [47], and IC_0 and k are calibration parameters that define the shape of the SDR-IC relationship as a Sigmoid function.

Finally, the sediment reaches the stream at the outlet of the Upper Ing watershed. The total sediment export was calculated from the sum of the amount of annual soil loss multiplied by the sediment delivery ratio [48]:

$$E = \sum_i E_i, \quad (7)$$

where E_i is the sediment that erodes from any LULC that reaches the stream.

3.5.2. Nutrient Export Estimation

Under the NDR model, the nutrient loads are first defined based on the LULC map and associated loading rates. Then, the model calculates LULC-based loads and the runoff potential index to approximate modified loads, which are divided into sediment-bound (surface flow) and dissolved parts (subsurface flow). After that, nutrient delivery is computed for surface NDR and subsurface NDR based on the properties of pixels belonging to the same flow path (particularly the slope and retention efficiency of the land use) [48].

The NDR model requires specific factors and parameters to run the model. Some factors in this model are the same as those in the SDR model, including DEM, LULC, TFA, and K_b . Other parameters, including nitrogen and phosphorus loads, nutrient runoff proxy, maximum retention efficiency, and critical length, were added. The specific required factors of the NDR models are summarized below.

(1) The nutrient runoff proxy (RP) is used to calculate the runoff potential index. The runoff proxy was interpolated, based on annual rainfall, using the inverse distance weighted (IDW) method.

(2) Land-use and land-cover (LULC) data represent the influence of the nutrient delivery to the stream. LULC data were used as input data to assign the nutrient loading for each LULC class (loads), as summarized in Table 4.

(3) The maximum retention efficiency (eff) indicates the proportion of nutrient retention by vegetation. The value for each LULC class varies between zero and one (see Table 4).

(4) The critical length (crit_len) is the distance that a patch of LULC retains nutrients in its maximum capacity. The critical length ranges from 10 to 300 m [49,50]. In this study, the value was first set to the pixel resolution, with a value of 30 m (see Table 4).

(5) The subsurface proportion (proportion_subsurface) value is the proportion of dissolved nutrients that travels by surface and subsurface flow. We set its value to zero, which indicates that all nutrients are delivered by surface flow (see Table 4).

After that, the NDR model was computed to transport nutrients by surface flow. The surface nutrient delivery ratio is the product of a delivery factor, representing the ability of downstream pixels to transport nutrients without retention, and was calculated using Equation (8) [48]:

$$NDR_i = \frac{NDR_{0,i}}{1 + \exp\left(\frac{IC_i - IC_0}{k}\right)}, \tag{8}$$

where $NDR_{0,i}$ is the proportion of a nutrient that is not retained by downstream pixels (which is based on the maximum retention efficiency of the land between a pixel and the stream), IC_i is a topographic index, and IC_0 and k are calibration parameters that define the shape of the NDR–IC relationship.

Finally, the total nutrient export at the outlet of the watershed is estimated, from the sum of the product of the load and the NDR [48], as:

$$x_{exp_{tot}} = \sum_i x_{exp_i}, \tag{9}$$

where x_{exp_i} is the nutrient export from any LULC, as the product of the load and the NDR.

Table 4. Data related to nitrogen, phosphorus, and related variables corresponding to each LULC class.

No	LULC Type	Nitrogen				Phosphorus			
		Load	Eff	Crit_len	Proportion_subsurface	Load	Eff	Crit_len	Proportion_subsurface
1	Urban	7.75	0.05	30	0	1.3	0.05	30	0
2	Paddy field	11	0.25	30	0	3	0.25	30	0
3	Field crop	11	0.25	30	0	3	0.25	30	0
4	Para rubber	10	0.45	30	0	3	0.45	30	0
5	Perennial trees and orchards	10	0.45	30	0	3	0.45	30	0
6	Forest area	1.8	0.7	30	0	0.011	0.7	30	0
7	Waterbody	0.001	0.05	30	0	0.001	0.05	30	0
8	Rangeland	2	0.5	30	0	0.011	0.5	30	0
9	Wetland	2	0.8	30	0	0.05	0.8	30	0
10	Miscellaneous land	4	0.05	30	0	0.001	0.05	30	0

Source: [25].

Furthermore, the performance of the SDR and NDR models was examined based on data observed by the PCD in the calibration period (2011–2015) and validation period (2016–2018) with standard scale, using the coefficient of determination (R^2) and percent bias ($PBIAS$), as suggested by [51,52] (see Equations (10) and (11) and Table 5).

$$R^2 = \left\{ \frac{\sum_{i=1}^n (X_s - \bar{X}_s)(X_o - \bar{X}_o)}{\left[\sum_{i=1}^n (X_s - \bar{X}_s)^2 \sum_{i=1}^n (X_o - \bar{X}_o)^2 \right]^{0.5}} \right\}^2, \tag{10}$$

where \bar{X}_o is the observed export value at station i , \bar{X}_o is the average of observed export value over the validation period, X_s is the simulated export value at station i , and \bar{X}_s is the average simulated export value over the validation period. Furthermore, i is the number of stations, and n is the total count of data pairs. The value of R^2 varies from 0 to 1.

$$PBIAS = \frac{\sum_{i=1}^n (X_i^o - X_i^s)}{\sum_{i=1}^n (X_i^o)} \times 100, \tag{11}$$

where X_i^o is an observed export value at time step i , and X_i^s is a simulated export value at time step i .

Table 5. Model performance scale.

Model Evaluation	Constituent	Performance Ratings			
		Unsatisfactory	Satisfactory	Good	Very Good
R^2	SS TP, TN	<0.5	0.5–0.6	0.6–0.7	0.7–1
$PBIAS$	SS	>55	30–55	15–30	<15
	TP, TN	>70	40–70	25–40	<25

Note: SS, suspended sediment; TP, total phosphorus, and TN, total nitrogen. Source: [51,52].

3.6. Suitable LULC Allocation Scenario to Minimize Sediment and Nutrient Export

To assess the state of change in ecosystem services (i.e., sediment and nutrient export due to LULC change), the ecosystem services change index (ESCI) was applied to assess the ecosystem service states (ES), as proposed by [27]:

$$ESCI_x = \left[\frac{ES_{CURx_j} - ES_{HISx_i}}{ES_{HISx_i}} \right], \tag{12}$$

where $ESCI_x$ is the ecosystem service change index of service x , and ES_{CURx_j} and ES_{HISx_i} are the current and historic ecosystem service state values of service x at times j and i , respectively.

In this study, the ecosystem service change indices of sediment and nutrient export ecosystem service values for LULC in 2019 (as the base year), and those of the predicted LULC between 2020 and 2029 were separately calculated in a pairwise manner using the ESCI, then averaged to identify the suitable LULC allocation under the proposed scenarios to minimize sediment or/and nutrient export.

4. Results

4.1. LULC Classification and LULC Change Detection

The results of LULC classification in 2009 and 2019 using the SVM algorithm are presented in Table 6 and Figure 3. As a result, the top three dominant LULC types in 2009 and 2019 were forest land, paddy field, and perennial trees and orchards. Meanwhile, the top three least dominant LULC types were miscellaneous land, para rubber, and rangeland in 2009 and miscellaneous land, wetland, and para rubber in 2019.

According to a simple comparison of LULC change in the area, the annual change rate and percentage of change between 2009 and 2019 are reported in Table 7. The dominant increasing areas of LULC types were perennial trees and orchards, para rubber, and rangeland, with annual change rates of 1.95, 1.64, and 1.05 km², respectively. Contrarily, the major decreasing areas of LULC classes in the same period were forest land and paddy fields, with annual change rates of 3.98 and 2.04 km², respectively. The primary cause of change areas was the conversion of paddy fields into perennial trees and orchards and the expansion of agricultural areas into forest land.

Table 6. Area and percentage of LULC data in 2009 and 2019.

No	LULC Type	2009		2019	
		km ²	Percentage	km ²	Percentage
1	Urban and built-up area	29.78	3.34	33.10	3.71
2	Paddy field	241.14	27.05	220.74	24.76
3	Field crop	17.49	1.96	21.84	2.45
4	Para rubber	3.35	0.38	19.78	2.22
5	Perennial trees and orchards	59.71	6.70	79.22	8.89
6	Forest land	476.73	53.48	436.91	49.02
7	Water body	26.06	2.92	33.37	3.74
8	Rangeland	16.75	1.88	27.26	3.06
9	Wetland	19.47	2.18	16.41	1.84
10	Miscellaneous land	0.87	0.10	2.71	0.30
Total		891.35	100	891.35	100

Table 7. Simple LULC change detection between 2009 and 2019.

LULC	LULC Type (Area, km ²)									
	UR	PD	FC	RP	PO	FO	WB	RL	WL	ML
In 2009	29.78	241.14	17.49	3.35	59.71	476.73	26.06	16.75	19.47	0.87
In 2019	33.10	220.74	21.84	19.78	79.22	436.91	33.37	27.26	16.41	2.71
Change area	3.32	−20.40	4.35	16.43	19.51	−39.82	7.31	10.51	−3.06	1.84
Annual change rate	0.33	−2.04	0.44	1.64	1.95	−3.98	0.73	1.05	−0.31	0.18
Percentage of change	0.37	−2.29	0.49	1.84	2.19	−4.47	0.82	1.18	−0.34	0.21

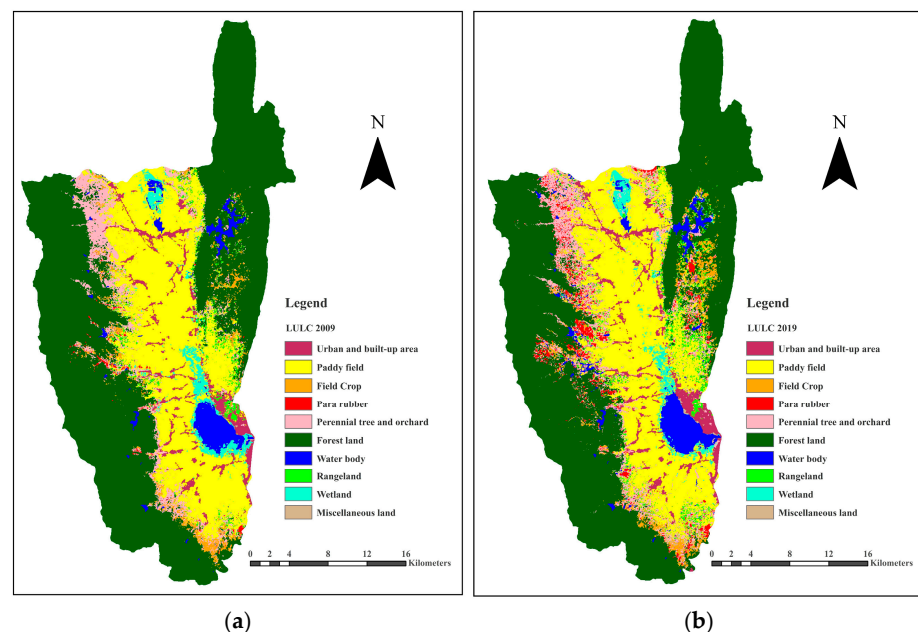


Figure 3. Spatial distribution of LULC classification in: (a) 2009 and (b) 2019.

4.2. Driving Factors of LULC Change

The multicollinearity test among the physical and socio-economic factors (independently available) was conducted using the VIF, as reported in Table A3 in Appendix B. As a result, all selected driving factors were found to be insignificantly correlated, as the VIF values did not exceed 10. They were further used to analyze specific LULC type location preferences by binary logistic regression analysis, as shown in Table 8.

Table 8. Multiple linear equations of each LULC type location preference and AUC value by binary logistic regression analysis.

Driving Forces	UR	PD	FC	RB	PO	FO	WA	RL	WL	ML
Constant	12.86	39.01	4.96	−3.06	−4.43	−29.41	3.27	3.68	26.41	4.78
Soil drainage (X_1)	−0.07	0.00	0.34	0.32	0.19	0.03	n. s.	0.34	−0.64	0.40
Distance to stream (X_2)	0.00	0.00	n. s.	n. s.	n. s.	n. s.	0.00	0.00	n. s.	n. s.
Distance to water body (X_3)	0.00	n. s.	n. s.	0.00	n. s.	n. s.	0.00	n. s.	0.00	n. s.
Distance to village (X_4)	0.00	n. s.	0.00	n. s.	n. s.	n. s.	n. s.	n. s.	n. s.	n. s.
Slope (X_5)	n. s.	−0.02	0.03	n. s.	−0.01	0.09	−0.14	0.02	−0.10	0.07
Distance to road (X_6)	−0.02	0.00	0.00	0.00	0.00	n. s.	0.00	0.00	n. s.	n. s.
Distance to fault line (X_7)	n. s.	n. s.	n. s.	n. s.	n. s.	n. s.	n. s.	n. s.	n. s.	n. s.
Annual rainfall (X_8)	n. s.	0.00	0.01	n. s.	0.00	0.00	0.00	0.00	0.01	0.01
Elevation (X_9)	−0.03	−0.10	n. s.	n. s.	0.00	0.06	0.01	0.01	−0.08	n. s.
Income per capita at subdistrict level (X_{10})	n. s.	n. s.	n. s.	n. s.	n. s.	n. s.	n. s.	n. s.	n. s.	n. s.
Population density at subdistrict level (X_{11})	0.00	0.00	0.01	0.01	n. s.	n. s.	n. s.	0.00	n. s.	n. s.
AUC	0.96	0.96	0.86	0.80	0.80	0.99	0.95	0.83	0.95	0.80

According to the result, the most significant driving factor for all LULC type allocation in the study area was soil drainage. The second most important vital driving factors were slope and annual rainfall. The third most crucial driving factors for the LULC type allocation area were distance to the road and elevation. In the meantime, other factors played crucial roles in specific LULC types, as shown in the table. Nevertheless, the distance to fault line and the income per capita at the subdistrict level were insignificant driving factors for all LULC type allocations in the study area.

4.3. Local Parameter of CLUE-S Model for LULC Prediction

The conversion matrix of LULC change for LULC prediction of three scenarios, which were assigned by considering the transition probability matrix of LULC data between 2009 and 2019 (Table 9), is presented in Tables 10–12. Meanwhile, elasticity values, as probability values for the urban and built-up area, paddy field, field crop, para rubber, perennial trees and orchards, forest land, waterbody, rangeland, wetland, and miscellaneous land were 1.00, 0.84, 0.22, 0.37, 0.67, 0.92, 0.93, 0.38, 0.45, and 0.29, respectively.

4.4. Land Requirement Estimation and LULC Prediction under Scenario I

The land requirement estimation for Scenario I (Trend of LULC evolution) was calculated based on the annual rate of LULC change from the transition area matrix between 2019 and 2029, using the Markov Chain model presented in Table 13. The significant increase in land requirements in the predictive period was observed in perennial trees and orchards, para rubber, water body, rangeland, urban and built-up area, field crop, and miscellaneous land. In contrast, the land requirements decreased for forest land, paddy field, and wetland.

Table 9. Transition probability matrix of LULC change between 2009 and 2019 by the Markov Chain model.

LULC Types	LULC in 2019									
	UR	PD	FC	RB	PO	FO	WB	RL	WL	ML
Urban and built-up area (UR)	1.000	-	-	-	-	-	-	-	-	-
Paddy field (PD)	0.005	0.842	0.001	0.012	0.068	-	0.010	0.037	0.025	0.002
Field crop (FC)	0.002	0.085	0.216	0.146	0.269	-	0.005	0.207	-	0.071
Para rubber (RB)	-	0.187	0.026	0.371	0.308	-	0.081	0.022	-	0.005
Perennial trees and orchards (PO)	0.002	0.086	0.029	0.096	0.667	-	0.029	0.087	-	0.004
Forest land (FO)	0.001	0.003	0.033	0.013	0.023	0.916	0.003	0.006	0.001	-
Water body (WB)	-	0.003	-	-	0.023	-	0.930	0.002	0.040	0.001
Rangeland (RL)	0.055	0.255	0.014	0.059	0.224	-	0.006	0.382	-	0.006
Wetland (WL)	0.010	0.253	-	0.002	0.095	-	0.166	0.007	0.452	0.016
Miscellaneous land (ML)	0.123	0.140	0.094	0.100	0.165	-	0.043	0.048	-	0.288

Table 10. Conversion matrix of possible LULC change between 2019 and 2029 for Scenario I (Trend of LULC evolution).

LULC Types	Possible Change in 2029									
	UR	PD	FC	RB	PO	FO	WB	RL	WL	ML
Urban and built-up area (UR)	1	0	0	0	0	0	0	0	0	0
Paddy field (PD)	1	1	0	0	0	0	0	1	0	1
Field crop (FC)	1	0	1	1	1	0	0	1	0	1
Para rubber (RB)	0	0	0	1	0	0	0	0	0	0
Perennial trees and orchards (PO)	0	0	0	1	1	0	0	0	0	0
Forest land (FO)	1	0	1	1	0	1	1	1	0	1
Water body (WB)	0	0	0	0	0	0	1	0	1	0
Rangeland (RL)	1	1	0	1	1	0	0	1	0	0
Wetland (WL)	0	1	0	0	0	0	1	0	1	1
Miscellaneous land (ML)	1	0	1	1	0	0	0	0	0	1

Note: 0 is not allowed, and 1 is allowed.

Table 11. Conversion matrix of possible LULC change between 2019 and 2029 for Scenario II (Maximization of ecosystem service values).

LULC Types	Possible Change in 2029									
	UR	PD	FC	RB	PO	FO	WB	RL	WL	ML
Urban and built-up area (UR)	1	0	0	0	0	0	0	0	0	0
Paddy field (PD)	1	1	0	0	0	0	0	1	1	1
Field crop (FC)	1	0	1	1	1	0	0	1	0	1
Para rubber (RB)	0	0	0	1	0	0	0	0	0	0
Perennial trees and orchards (PO)	0	0	0	1	1	0	0	0	0	0
Forest land (FO)	1	0	1	1	0	1	1	1	0	1
Water body (WB)	0	0	0	0	0	0	1	0	0	0
Rangeland (RL)	1	1	0	1	1	0	0	1	1	0
Wetland (WL)	0	1	0	0	0	0	0	0	1	1
Miscellaneous land (ML)	1	0	1	1	0	0	0	0	1	1

Note: 0 is not allowed, and 1 is allowed.

The results of LULC prediction data for Scenario I, which were simultaneously allocated based on elasticity values and conversion matrix of LULC change (Tables 9 and 10), the land requirements (Table 13), and driving factors on LULC change for specific LULC type location preference (Table 8), are presented in Table 14 and Figure 4. Meanwhile, the deviation between the estimated land requirements and predicted LULC data in 2029 under Scenario I is reported in Table A4 in Appendix B.

Table 12. Conversion matrix of possible LULC change between 2019 and 2029 for Scenario III (Economic crop zonation).

LULC Types	Possible Change in 2029									
	UR	PD	FC	RB	PO	FO	WB	RL	WL	ML
Urban and built-up area (UR)	1	0	0	0	0	0	0	0	0	0
Paddy field (PD)	1	1	0	0	0	0	0	1	0	1
Field crop (FC)	1	0	1	0	0	0	0	1	0	1
Para rubber (RB)	0	0	1	1	0	0	0	0	0	0
Perennial trees and orchards (PO)	0	0	1	1	1	0	0	0	0	0
Forest land (FO)	1	1	1	1	1	1	1	1	0	1
Water body (WB)	0	0	0	0	0	0	1	0	1	0
Rangeland (RL)	1	1	1	0	0	0	0	1	0	0
Wetland (WL)	0	1	0	0	0	0	1	0	1	1
Miscellaneous land (ML)	1	1	1	0	0	0	0	1	0	1

Note: 0 is not allowed, and 1 is allowed.

Table 13. Annual land requirements under Scenario I for each LULC type.

Year	Area (in km ²)									
	UR	PD	FC	RB	PO	FO	WB	RL	WL	ML
2019	33.10	220.74	21.84	19.78	79.22	436.91	33.37	27.26	16.41	2.71
2020	33.48	219.75	21.94	20.65	81.18	433.26	34.16	27.87	16.25	2.81
2021	33.86	218.77	22.03	21.52	83.13	429.61	34.96	28.48	16.09	2.91
2022	34.24	217.78	22.13	22.38	85.08	425.96	35.76	29.09	15.93	3.01
2023	34.63	216.79	22.22	23.25	87.03	422.30	36.56	29.70	15.77	3.11
2024	35.01	215.80	22.32	24.12	88.98	418.65	37.35	30.31	15.60	3.21
2025	35.39	214.82	22.41	24.98	90.93	415.00	38.15	30.92	15.44	3.30
2026	35.77	213.83	22.51	25.85	92.89	411.34	38.95	31.53	15.28	3.40
2027	36.16	212.84	22.60	26.71	94.84	407.69	39.75	32.14	15.12	3.50
2028	36.54	211.85	22.70	27.58	96.79	404.04	40.54	32.75	14.96	3.60
2029	36.92	210.86	22.79	28.45	98.74	400.38	41.34	33.36	14.80	3.70
Annual rate	0.38	−0.99	0.10	0.87	1.95	−3.65	0.80	0.61	−0.16	0.10

Table 14. Area of predicted LULC between 2020 and 2029 under Scenario I.

LULC Types	Area (in km ²)									
	2020	2021	2022	2023	2024	2025	2026	2027	2028	2029
Urban and built-up area	33.45	33.83	34.19	34.61	34.99	35.39	35.76	36.15	36.50	36.90
Paddy field	219.73	218.73	217.73	216.77	215.77	214.81	213.81	212.79	211.82	210.84
Field crop	21.94	22.04	22.13	22.23	22.31	22.43	22.51	22.58	22.69	22.81
Para rubber	20.65	21.53	22.42	23.26	24.10	24.99	25.86	26.69	27.57	28.45
Perennial trees and orchards	81.17	83.14	85.12	87.04	88.95	90.94	92.89	94.82	96.77	98.75
Forest land	433.27	429.62	425.96	422.30	418.63	415.00	411.35	407.68	404.03	400.39
Water body	34.18	34.99	35.78	36.57	37.36	38.16	38.97	39.76	40.58	41.35
Rangeland	27.86	28.48	29.10	29.70	30.29	30.91	31.52	32.13	32.72	33.36
Wetland	16.31	16.10	15.95	15.79	15.76	15.44	15.30	15.27	15.10	14.82
Miscellaneous land	2.79	2.88	2.98	3.08	3.19	3.28	3.38	3.48	3.57	3.68
Total	891.35	891.35	891.35	891.35	891.35	891.35	891.35	891.35	891.35	891.35

As a result, the LULC prediction between 2020 and 2029 was determined in terms of the driving factors of LULC change and local parameters (conversion matrix and elasticity values), particularly land requirements, which were estimated based on the transition area matrix between 2019 and 2029 using the Markov Chain model. The derived predicted LULC data correspond to the definition of Scenario I, which allows for LULC change (decreased or increased area) according to the trend of LULC evolution from 2009 to 2019, to represent socio-economic development in the study area.

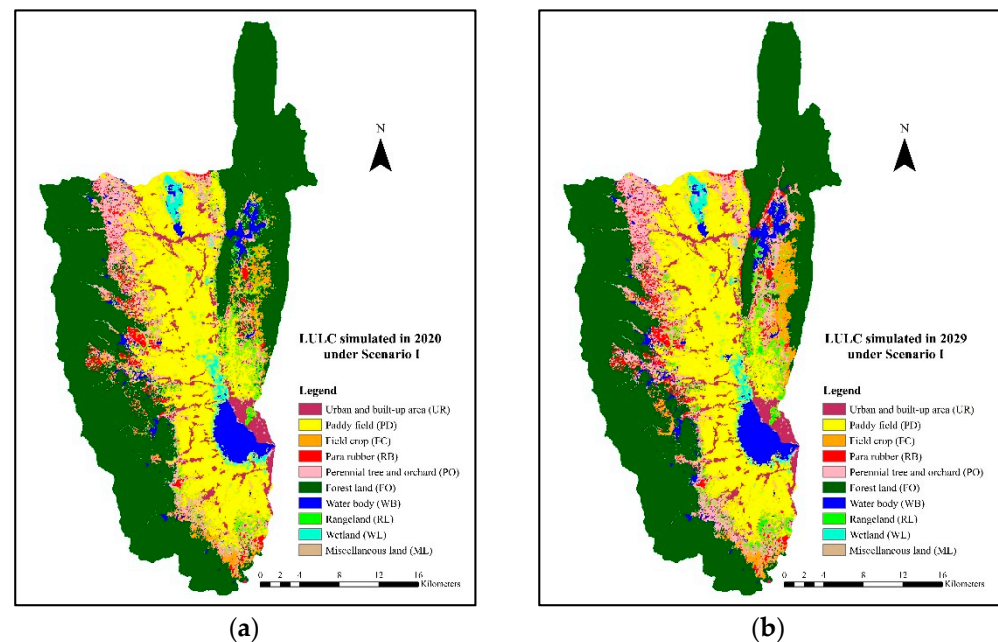


Figure 4. Spatial distribution of LULC data under Scenario I: (a) in 2020 and (b) in 2029.

There was a slight difference between the required land area and the predicted area of each LULC type in 2029 under Scenario I (see Table A4 in Appendix B). The deviation values varied between -0.0002% (0.02 km^2 ; underestimation) to 0.0002% (0.02 km^2 ; overestimation). The deviation values depend on the iterative driving factor that determines the highest probability that each spatial unit will be converted to a specific land-use type in the following year [53,54]. Nevertheless, the summation of deviation values (i.e., considering the trade-off between overestimation and underestimation among LULC types) was 0.00% . Therefore, the LULC prediction under Scenario I can be considered acceptable for estimating sediment and nutrient export in the study area.

4.5. Land Requirement Estimation and LULC Prediction under Scenario II

The land requirement estimation under Scenario II (Maximization of ecosystem service values), which was estimated based on the annual rate change between classified LULC data in 2019 and allocated LULC data in 2029 after maximization of ecosystem services according to the objective function (see Equation (1)) and constraining decision variables (see Table A5 in Appendix B) using LP through the Simplex method, is reported in Table 15.

As a result, the increased LULC classes under this scenario were urban and built-up area, para rubber, perennial trees and orchards, and wetland, with increasing annual rates of 0.38 , 0.87 , 1.95 , and 1.34 km^2 , respectively. In contrast, the decreased LULC classes in 2029 were paddy fields, forest land, rangeland, and miscellaneous land, with annual rates of decrease of 0.99 , 2.06 , 1.36 , and 0.14 km^2 , respectively. Meanwhile, field crops and water bodies were unchanged.

The results of LULC prediction data between 2020 and 2029 under Scenario II, which were simultaneously allocated based on elasticity values and the conversion matrix of LULC change (Tables 9 and 11), the land requirements (Table 15), and driving factors of LULC change for specific LULC type location preference (Table 8), are presented in Table 16 and Figure 5. Meanwhile, the deviation between the estimated land requirements and predicted LULC data in 2029 under Scenario II is reported in Table A6 in Appendix B.

Table 15. Annual land requirements under Scenario II for each LULC type.

Year	Area (in km ²)									
	UR	PD	FC	RB	PO	FO	WA	RL	WL	ML
2019	33.10	220.74	21.84	19.78	79.22	436.91	33.37	27.26	16.41	2.71
2020	33.48	219.75	21.84	20.65	81.18	434.86	33.37	25.90	17.75	2.58
2021	33.86	218.77	21.84	21.52	83.13	432.80	33.37	24.54	19.10	2.44
2022	34.24	217.78	21.84	22.38	85.08	430.74	33.37	23.17	20.44	2.31
2023	34.63	216.79	21.84	23.25	87.03	428.68	33.37	21.81	21.79	2.17
2024	35.01	215.80	21.84	24.12	88.98	426.62	33.37	20.45	23.13	2.03
2025	35.39	214.82	21.84	24.98	90.93	424.56	33.37	19.08	24.48	1.90
2026	35.77	213.83	21.84	25.85	92.89	422.50	33.37	17.72	25.82	1.76
2027	36.16	212.84	21.84	26.71	94.84	420.44	33.37	16.36	27.17	1.63
2028	36.54	211.85	21.84	27.58	96.79	418.38	33.37	14.99	28.51	1.49
2029	36.92	210.86	21.84	28.45	98.74	416.32	33.37	13.63	29.85	1.36
Annual Change rate	0.38	−0.99	0.00	0.87	1.95	−2.06	0.00	−1.36	1.34	−0.14

Note: Annual change rate was calculated based on the classified LULC data in 2010 by SVM and allocated LULC area to maximize ecosystem service by LP.

Table 16. Area of predicted LULC between 2020 and 2029 under Scenario II.

LULC Types	Area (in km ²)									
	2020	2021	2022	2023	2024	2025	2026	2027	2028	2029
Urban and built-up area	33.36	33.84	34.22	34.60	34.99	35.39	35.42	36.17	36.47	36.94
Paddy field	219.74	218.73	217.75	216.77	215.78	214.77	213.82	212.74	211.81	210.78
Field crop	21.85	21.82	21.82	21.81	21.81	21.86	21.85	21.84	21.86	21.80
Para rubber	20.67	21.50	22.37	23.23	24.09	24.98	25.87	26.74	27.56	28.46
Perennial trees and orchards	81.16	83.12	85.05	87.01	88.96	90.81	92.90	94.81	96.70	98.68
Forest land	434.86	432.77	430.71	428.65	426.61	424.52	422.49	420.45	418.34	416.34
Water body	33.57	33.57	33.57	33.57	33.57	33.70	33.70	33.70	33.70	33.70
Rangeland	25.87	24.51	23.16	21.78	20.43	19.14	17.72	16.35	14.97	13.57
Wetland	17.72	19.07	20.42	21.76	23.10	24.27	25.82	26.93	28.44	29.72
Miscellaneous land	2.56	2.42	2.29	2.15	2.02	1.89	1.77	1.62	1.48	1.36
Total	891.35	891.35	891.35	891.35	891.35	891.35	891.35	891.35	891.35	891.35

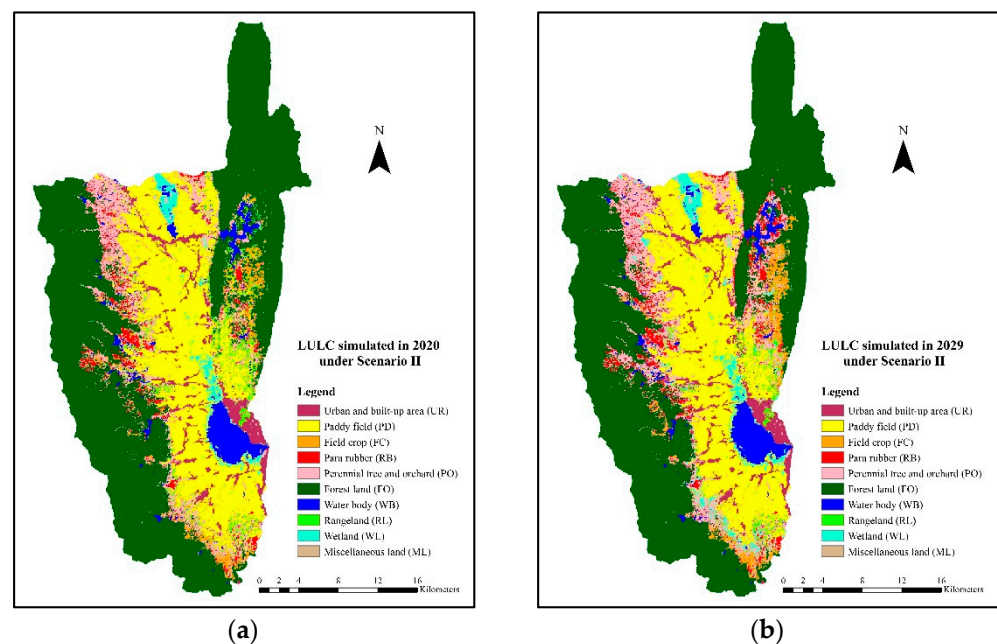


Figure 5. Spatial distribution of LULC data under Scenario II: (a) in 2020 and (b) in 2029.

As a result, the significant LULC types with increasing area were urban and built-up area, para rubber, perennial trees/orchards, water body, and wetlands, but the several LULC types with decreased area were paddy fields, field crops, forest land, rangeland, and miscellaneous land. In particular, wetland—which provides the highest coefficient value for ecosystem services—is expected to increase in the future. Wetland areas increased from 16.41 km² in 2019 to 29.72 km² in 2029, coming from paddy fields (9.50 km²), rangeland (2.83 km²), and miscellaneous land (0.98 km²) in 2019. This result implies the efficacy of linear programming for determining reclaimed and other areas changing into the wetland.

Like Scenario I, there was a slight difference between the required land area and the predicted area of each LULC type in 2029 under Scenario II. The deviation values varied from −0.0013 to 0.0033%; nevertheless, the summation of deviation values was 0.00%. (See Table A6 in Appendix B). Hence, the LULC prediction under Scenario II can be considered acceptable for estimating sediment and nutrient export in the study area.

4.6. Land Requirement Estimation and LULC Prediction under Scenario III

Land requirement estimation under Scenario III (Economic crop zonation) was estimated based on areas of suitability classes for economic crops according to the LDD and Markov Chain model, as shown in Table 17.

As a result, the increased LULC classes were paddy field, field crop, water body, rangeland, urban and built-up area, and miscellaneous land, with annual increase rates of 5.96, 1.21, 0.80, 0.61, 0.38, and 0.10 km², respectively. In contrast, the decreased LULC classes were perennial trees and orchards, forest land, wetland, and para rubber, with annual decrease rates of 5.23, 3.65, 0.16, and 0.01 km², respectively.

The results of LULC prediction data between 2020 and 2029 under Scenario III, which were simultaneously allocated based on elasticity values and the conversion matrix of LULC change (Tables 9 and 12), the land requirements (Table 17), and driving factors of LULC change for specific LULC type location preference (Table 8), are presented in Table 18 and Figure 6. In the meantime, the deviation between the estimated land requirements and predicted LULC data in 2029 under Scenario III is reported in Table A7 in Appendix B.

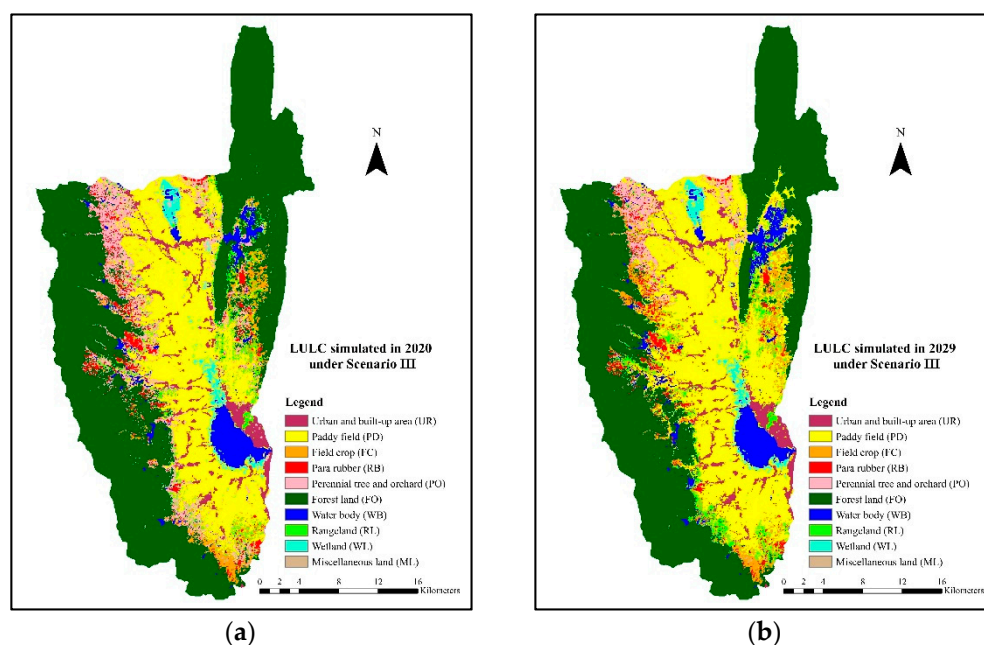
Table 17. Annual land requirements under Scenario III for each LULC type.

Year	Area (in km ²)									
	UR	PD	FC	RB	PO	FO	WA	RL	WL	ML
2019	33.10	220.74	21.84	19.78	79.22	436.91	33.37	27.26	16.41	2.71
2020	33.48	226.70	23.05	19.77	73.99	433.26	34.16	27.87	16.25	2.81
2021	33.86	232.66	24.26	19.76	68.76	429.61	34.96	28.48	16.09	2.91
2022	34.24	238.62	25.48	19.75	63.52	425.96	35.76	29.09	15.93	3.01
2023	34.63	244.58	26.69	19.74	58.29	422.30	36.56	29.70	15.77	3.11
2024	35.01	250.54	27.90	19.72	53.05	418.65	37.35	30.31	15.60	3.21
2025	35.39	256.50	29.11	19.71	47.82	415.00	38.15	30.92	15.44	3.30
2026	35.77	262.46	30.32	19.70	42.58	411.34	38.95	31.53	15.28	3.40
2027	36.16	268.42	31.53	19.69	37.35	407.69	39.75	32.14	15.12	3.50
2028	36.54	274.38	32.74	19.68	32.12	404.04	40.54	32.75	14.96	3.60
2029	36.92	280.34	33.96	19.66	26.88	400.38	41.34	33.36	14.80	3.70
Annual Change rate	0.38	5.96	1.21	−0.01	−5.23	−3.65	0.80	0.61	−0.16	0.10

As a result, under Scenario III, economic crop areas, precisely paddy field, field crop, para rubber, and perennial trees and orchards were located based on suitability classes of economic crop zonation. Paddy fields expanded from 220.74 km² in 2019 to 280.20 km² in 2029, and field crop areas increased from 21.84 km² in 2019 to 34.11 km² in 2029. Meanwhile, areas of para rubber were unchanged in 2029, with an area of 19.78 km². To the contrary, perennial trees and orchards are expected to decrease from 79.22 km² in 2019 to 26.94 km². This result indicates the influence of economic crop zonation on LULC prediction under Scenario III.

Table 18. Area of predicted LULC between 2020 and 2029 under Scenario III.

LULC Types	Area (in km ²)									
	2020	2021	2022	2023	2024	2025	2026	2027	2028	2029
Urban and built-up area	33.20	33.78	33.94	34.56	34.76	35.41	35.75	36.10	36.65	36.96
Paddy field	226.72	232.67	238.65	244.54	250.55	256.39	262.42	268.46	274.37	280.20
Field crop	23.08	24.26	25.54	26.74	27.93	29.15	30.40	31.62	32.79	34.11
Para rubber	19.78	19.83	19.85	19.87	19.89	19.89	19.89	19.88	19.59	19.78
Perennial trees and orchards	74.06	68.78	63.62	58.31	53.13	47.91	42.65	37.46	32.17	26.94
Forest land	433.30	429.61	425.98	422.30	418.60	414.93	411.24	407.57	403.96	400.22
Water body	34.34	34.93	35.73	36.43	37.07	37.96	38.71	39.48	40.47	41.11
Rangeland	27.86	28.46	29.06	29.68	30.61	30.94	31.56	32.14	32.78	33.44
Wetland	16.22	16.10	15.97	15.78	15.63	15.43	15.29	15.11	14.96	14.85
Miscellaneous land	2.79	2.92	3.00	3.14	3.18	3.34	3.44	3.53	3.61	3.73
Total	891.35	891.35	891.35	891.35	891.35	891.35	891.35	891.35	891.35	891.35

**Figure 6.** Spatial distribution of LULC data under Scenario III: (a) in 2020 and (b) in 2029.

As with Scenario I, there was a slight difference between the required land area and the predicted area of each LULC type in 2029 under Scenario III. The deviation values varied from -0.0023 to 0.0015% ; however, the summation of deviation values was 0.00% . (See Table A7 in Appendix B). Hence, the LULC prediction under Scenario III can be considered acceptable for estimating sediment and nutrient export in the study area.

4.7. Sediment Export Estimation Using SDR Model

In general, the SDR model reports soil erosion, sediment retention, sediment deposition, and sediment export. For this study, sediment export was selected to describe ecosystem services in the study area by each LULC allocation scenario (Scenarios I–III).

The statistical performance of the model under the calibration and validation periods provided a high correlation between the observed and estimated sediment export, with R^2 values of 0.697 and 0.824 , respectively, indicating the good and very good fitting performance rate of the model for nitrogen export estimation, as suggested by [51,52]. These findings are consistent with the previous study of [55], who applied the SDR model to analyze sediment at the Rmel river basin, and found that the correlation between the estimated and observed sediment export in the calibration process was relatively high, with R^2 values of 0.84 and 0.706 .

Meanwhile, the PBIAS values under the calibration period provided a good fit between the estimated and observed sediment export, with a value of -27.03% , while the PBIAS value under the validation period delivered an unsatisfactory fit between the estimated and observed sediment export, with a value of 65.60% , in accordance with [51,52]. The optimum local model parameters and domain values under the calibration period of the SDR model are summarized in Table 19.

Table 19. Systematic model parameters and optimum value under calibration period.

Parameter	Default Value	Minimum Value	Maximum Value	Adjusted Value	Optimum Value
K_b	2	1	2	0.5	1
IC_0	0.5	0.1	1	0.1	1
TFA	1000	1000	1800	200	1800

4.7.1. Sediment Export Estimation of Actual LULC in 2019

The sediment export in 2019 was about 26,421 tons or 29.64 tons/km². Additionally, the contribution of LULC type in 2019 to sediment export is presented in Table 20.

Table 20. Contribution of LULC type in 2019 to sediment exports.

LULC Types	Area (km ²)	Sediment Export		%
		Total (tons)	Average (tons/km ²)	
Urban and built-up area (UR)	33.10	-	-	-
Paddy field (PD)	220.70	2471.12	11.19	0.80
Field crop (FC)	21.84	7169.79	328.26	23.57
Para rubber (RB)	19.78	2555.61	129.18	9.27
Perennial trees and orchards (PO)	79.22	11,578.36	146.15	10.49
Forest land (FO)	436.90	246.47	0.56	0.04
Water body (WB)	33.37	-	-	-
Rangeland (RL)	27.26	323.29	11.86	0.85
Wetland (WL)	16.41	-	-	-
Miscellaneous land (ML)	2.71	2076.77	765.57	54.97
Total	891.4	26,421.41		100

As a result, the highest sediment export occurred on miscellaneous land, with an average value of 765.57 tons/km² (54.97%), while the lowest sediment export came from forest land, with a value of 0.56 tons/km² (0.04%). Additionally, urban and built-up areas, water bodies, and wetlands do not create sediment export, according to the C and P coefficients in the biophysical table.

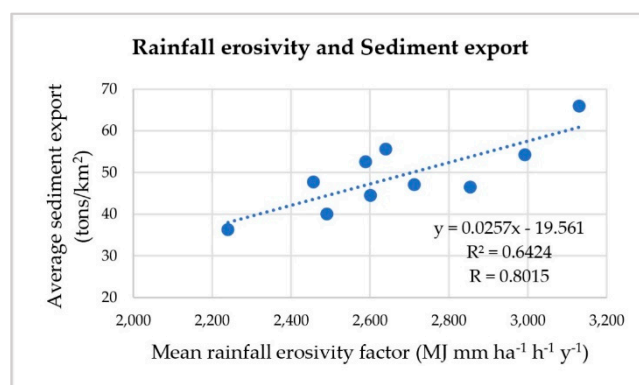
4.7.2. Sediment Export Estimation of Predicted LULC under Scenario I

Estimates of total and average sediment export under the predicted LULC between 2020 and 2029 under Scenario I (Trend of LULC evolution) and mean rainfall erosivity are presented in Table 21. As a result, the highest total and average sediment exports were about 58,798 tons and 65.97 tons/km², respectively, in 2026. The lowest total and average sediment exports were about 32,373 tons and 36.32 tons/km², respectively, in 2022.

Table 21. Estimation of sediment export between 2020 and 2029 under Scenario I.

Year	Sediment Export		Mean Rainfall Erosivity
	Total (tons)	Average (tons/km ²)	(MJ mm ha ⁻¹ h ⁻¹ y ⁻¹)
2020	41,445.02	46.50	2854.33
2021	35,685.45	40.04	2490.34
2022	32,373.49	36.32	2239.93
2023	41,954.52	47.07	2711.93
2024	39,669.68	44.51	2601.06
2025	48,329.18	54.22	2992.66
2026	58,797.97	65.97	3130.43
2027	42,549.03	47.74	2456.18
2028	46,867.05	52.58	2588.82
2029	49,558.85	55.60	2640.18
Average	43,723.02	49.06	2670.59

These results indicate that the primary influence of rainfall erosivity and LULC types in the RUSLE model affect sediment export, as has been suggested by many researchers [56–60]. The influence of rainfall erosivity on sediment export in this study was confirmed by simple linear regression analysis, resulting in Figure 7, with an R^2 value of 0.6424. This finding indicates that rainfall erosivity can explain the linear relationship with the sediment export by about 64%.

**Figure 7.** Relationship between mean rainfall erosivity and average sediment export under Scenario I.

Moreover, the contribution of the predicted LULC under Scenario I on sediment export between 2020 and 2029 indicated that miscellaneous land caused the highest average sediment export, with values between 819.56 tons/km² in 2022 and 1501.94 tons/km² in 2026. Meanwhile, forest land generated the lowest average sediment export, with values between 0.65 tons/km² in 2022 and 1.05 tons/km² in 2026.

4.7.3. Sediment Export Estimation of Predicted LULC under Scenario II

The estimated total and average sediment export under predicted LULC between 2020 and 2029 and mean rainfall erosivity, according to Scenario II (Maximization of ecosystem service values), are presented in Table 22. As a result, the highest total and average sediment exports were about 48,115 tons and 53.98 tons/km², respectively, in 2026. The lowest total and average sediment exports were about 30,190 tons and 33.87 tons/km², respectively, in 2022.

As with Scenario I, these results indicated that the primary influence of the rainfall erosivity factor and LULC types in the RUSLE model affected sediment export. The influence of rainfall erosivity on sediment export under Scenario II was relatively stronger than that in Scenario I, as shown in Figure 8. According to the R^2 value of 0.9589, the rainfall erosivity can explain the linear relationship with sediment export by about 96%.

Moreover, the contribution of the predicted LULC under Scenario II to sediment export between 2020 and 2029 revealed that miscellaneous land decreased every year under this scenario; still, it caused the highest average sediment export until 2027, with values between 1088.47 tons/km² in 2020 and 512.54 tons/km² in 2027. After that, the field crop yielded the highest average sediment export in 2028 and 2029, with values between 447.46 tons/km² and 470.16 tons/km², respectively. In contrast, forest land generated the lowest average sediment export with values between 0.64 tons/km² in 2022 and 1.02 tons/km² in 2026.

Table 22. Estimation of sediment export between 2020 and 2029 under Scenario II.

Year	Sediment Export		Mean Rainfall Erosivity (MJ mm ha ⁻¹ h ⁻¹ y ⁻¹)
	Total (tons)	Average (tons/km ²)	
2020	40,979.13	45.97	2854.33
2021	34,149.06	38.31	2490.34
2022	30,190.61	33.87	2239.93
2023	38,483.96	43.17	2711.93
2024	35,659.13	40.01	2601.06
2025	41,526.64	46.59	2992.66
2026	48,115.01	53.98	3130.43
2027	33,851.75	37.98	2456.18
2028	36,216.79	40.63	2588.82
2029	37,599.82	42.18	2640.18
Average	37,677.19	42.27	2670.59

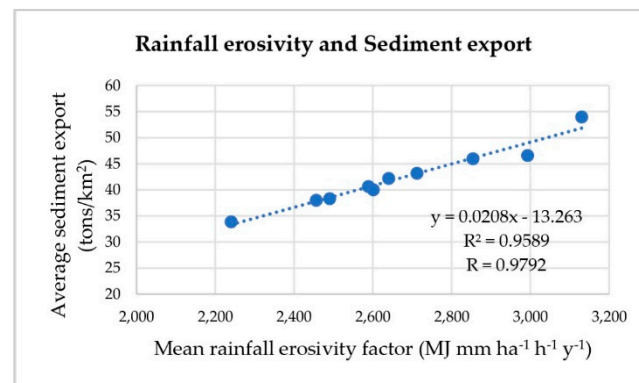


Figure 8. Relationship between mean rainfall erosivity and average sediment export under Scenario II.

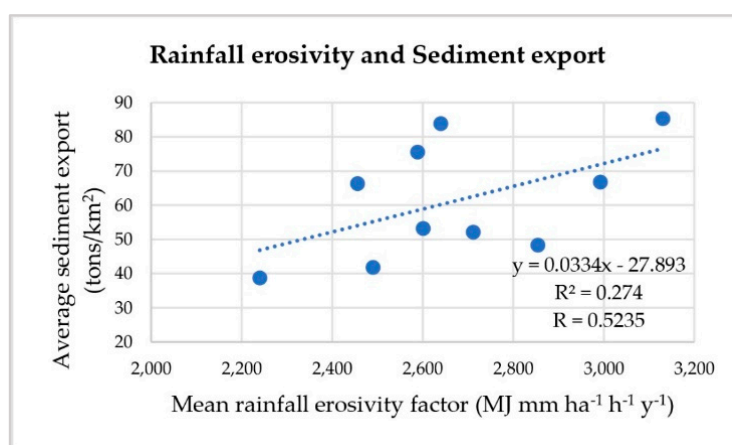
4.7.4. Sediment Export Estimation of Predicted LULC under Scenario III

The estimated total and average sediment export under the predicted LULC between 2020 and 2029 and mean rainfall erosivity according to Scenario III (Economic crop zonation) are presented in Table 23. As a result, the highest total and average sediment exports were about 76,068 tons and 85.34 tons/km², respectively, in 2026. The lowest total and average sediment exports are about 34,520 tons and 38.73 tons/km², respectively, in 2022.

As with Scenario I, these results indicate that the primary influence of rainfall erosivity factor and LULC types in the RUSLE model affected sediment export; however, the influence of rainfall erosivity on sediment export under Scenario III was lower than that under Scenario I, as shown in Figure 9. The simple linear equation indicates a moderately positive correlation between the mean rainfall erosivity factor and average sediment export under Scenario III, with an R value of 0.5235 and R² value of 0.274. According to the R² value, the rainfall erosivity can explain the linear relationship with sediment export by only 27%.

Table 23. Estimation of sediment export between 2020 and 2029 under Scenario III.

Year	Sediment Export		Mean Rainfall Erosivity (MJ mm ha ⁻¹ h ⁻¹ y ⁻¹)
	Total (tons)	Average (tons/km ²)	
2020	43,130.50	48.39	2854.33
2021	37,330.55	41.88	2490.34
2022	34,520.48	38.73	2239.93
2023	46,451.16	52.11	2711.93
2024	47,447.38	53.23	2601.06
2025	59,526.42	66.78	2992.66
2026	76,068.33	85.34	3130.43
2027	59,092.34	66.30	2456.18
2028	67,376.26	75.59	2588.82
2029	74,740.75	83.85	2640.18
Average	54,568.42	61.22	2670.59

**Figure 9.** Relationship between mean rainfall erosivity and average sediment export under Scenario III.

The contribution of the predicted LULC under Scenario III to sediment export between 2020 and 2029 reveals that miscellaneous land caused the highest average sediment export, with values between 1658.33 tons/km² in 2022 and 7372.09 tons/km² in 2029, while forest land generated the lowest average sediment export, with values between 0.65 tons/km² in 2022 and 1.08 tons/km² in 2026.

The average sediment export between 2020 and 2029 under the three scenarios was then compared, as shown in Figure 10, which shows that the predicted LULC under Scenario II (Maximization of ecosystem service values) delivered the lowest annual sediment export, compared to Scenarios I and III, with an average value of 42.27 tons/km² due to the increasing areas of wetland and decreasing areas of rangeland and miscellaneous land. In contrast, the areas of miscellaneous land in scenarios I and III were increased, based on the annual change rate of the Markov chain model. Though miscellaneous land showed only a minor increase, it caused high soil loss and sediment export.

Moreover, Scenario III delivered the highest annual sediment export when compared to the other scenarios, as the paddy field and field crop areas increased, according to economic crop zonation by the LDD in 2018.

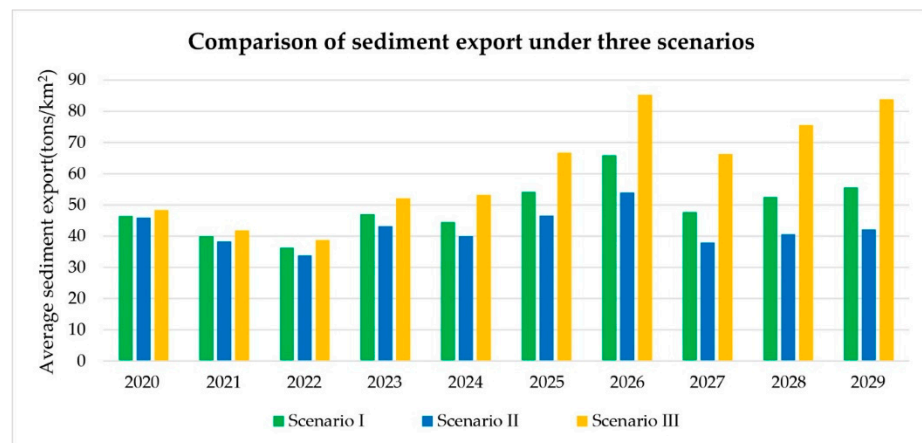


Figure 10. Comparison of sediment export between 2020 and 2029 under the three considered scenarios.

4.8. Nutrient Export Estimation Using NDR Model

Similar to sediment export, nutrient (N and P) exports were selected to describe ecosystem services in the study area by each LULC allocation scenario (Scenarios I–III).

The statistical performance of the NDR model for nitrogen export estimation under the calibration and validation periods showed satisfactory and very good fitting between the observed and estimated nitrogen export, with R² values of 0.575 and 0.895, respectively. At the same time, the PBIAS values under the calibration period provided a very good fit performance rate of the model, with a value of −20.42%, and PBIAS values under the validation period provided a good fit performance rate, with a value of 33.39%, in accordance with [51,52].

Meanwhile, the statistical NDR model performance for calibration and validation of phosphorus export provided a very good and good fit between the observed and estimated phosphorus export, with R² values of 0.828 and 0.643, respectively. At the same time, the PBIAS values for calibration and validation provided very good and good fitting performance rates of the model, with values of 12.57 and 30.21%, respectively, in accordance with [51,52]. The optimum local model parameters and domain values under the calibration period of the NDR model are summarized in Tables 24 and 25.

Table 24. Nutrient delivery ratio model parameters for model calibration.

Parameter	Default Value	Minimum Value	Maximum Value	Adjusted Value	Optimum Value
<i>K_b</i>	2	1	2	0.5	1
<i>TFA</i>	1000	1000	1800	200	1800
<i>load_n</i>	By LULC ¹ (See Table 4)	0.5×	3×	0.5×	By LULC (Table 25)
<i>eff_n</i>	By LULC ² (See Table 4)	0.5×	1×	0.5×	By LULC (Table 25)
<i>crit_{len_n}</i>	30 m ³	30	10×	5×	150
<i>load_p</i>	By LULC ² (See Table 4)	0.5×	3×	0.5×	By LULC (Table 25)
<i>eff_p</i>	By LULC ² (See Table 4)	0.5×	1×	0.5×	By LULC (Table 25)
<i>crit_{len_p}</i>	30 m ³	30	10×	5×	150

Note: ¹ *load_n* can be added from default values of all LULC types; ² *eff_n*, *eff_p*, *load_p*, can be added from default values only LULC types outside WWTF; ³ *crit_{len_n}* and *crit_{len_p}* can be added from default values only LULC types outside WWTF.

Table 25. Adjusted parameter of NDR model for nitrogen and phosphorus calibration.

LULC Types	load_n	eff_n	crit_len_n	load_p	eff_p	crit_len_p
Urban and built-up area	23.25	0.05	30	1.3	0.05	30
Paddy field	33	0.25	150	9	0.25	150
Field crop	33	0.25	150	9	0.25	150
Para rubber	30	0.45	150	9	0.45	150
Perennial trees and orchards	30	0.45	150	9	0.45	150
Forest land	5.4	0.7	150	0.033	0.7	150
Water body	0.003	0.05	150	0.003	0.05	150
Rangeland	6	0.5	150	0.033	0.5	150
Wetland	6	0.8	30	0.05	0.8	30
Miscellaneous land	12	0.05	150	0.003	0.05	150

4.8.1. Nutrient Export Estimation of Actual LULC in 2019

The estimated total and average nutrient (N and P) load and export of actual LULC in 2019 are presented in Table 26. Meanwhile, the amount of nutrient export from each LULC type in 2019 is presented in Table 27.

As a result, the total nitrogen and phosphorus loads in 2019 were about 1,422,800 kg (1596.23 kg/km²) and about 308,268 kg (345.84 kg/km²), and the total nitrogen and phosphorus exports were about 193,308 kg (216.87 kg/km²) and about 41,979 kg (47.10 kg/km²), respectively.

Table 26. Nutrient (N and P) load and export of actual LULC in 2019.

Total N load	1,422,800.13	(kg/year)
Total P load	308,267.70	(kg/year)
Average N load	1596.23	(kg/watershed in km ²)
Average P load	345.84	(kg/watershed in km ²)
Total N export	193,307.56	(kg/year)
Total P export	41,978.66	(kg/year)
Average N export	216.87	(kg/watershed in km ²)
Average P export	47.10	(kg/watershed in km ²)
Watershed area	891.35	Km ²

Table 27. Contribution of LULC type on nutrient (N and P) export in 2019.

LULC Types	Area	Nitrogen Export			Phosphorus Export		
	km ²	Total (kg)	Average (kg/km ²)	%	Total (kg)	Average (kg/km ²)	%
Urban and built-up area	33.10	8965.07	270.89	11.5	501.27	15.15	3.02
Paddy field	220.74	95,828.98	434.12	18.5	26,135.18	118.40	23.6
Field crop	21.84	9919.11	454.14	19.3	2705.21	123.86	24.7
Para rubber	19.78	7613.26	384.82	16.4	2283.98	115.45	23.0
Perennial trees and orchards	79.22	33,756.21	426.09	18.2	10,126.86	127.83	25.5
Forest land	436.91	34,402.68	78.74	3.35	210.24	0.48	0.10
Water body	33.37	2.22	0.07	0.0	2.22	0.07	0.01
Rangeland	27.26	1860.71	68.25	2.91	10.23	0.38	0.07
Wetland	16.41	398.40	24.28	1.03	3.32	0.20	0.04
Miscellaneous land	2.71	560.91	206.77	8.81	0.14	0.05	0.01
Total	891.4	193,307.56		100	41,978.66		100

In the meantime, the highest total nitrogen and phosphorus exports occurred at the paddy field, with values of about 95,829 and 26,135 kg, respectively. In contrast, the lowest total nitrogen export came from waterbody areas, with a value of 2.22 kg, and the lowest

total phosphorus export came from miscellaneous land, with a value of 0.14 kg. However, the highest average nitrogen and phosphorus export appeared on field crop and perennial trees and orchards, with values of 454.14 and 127.83 kg/km², respectively.

4.8.2. Nutrient Export Estimation of Predicted LULC under Scenario I

The estimated total and average nitrogen and phosphorus export of predicted LULC between 2020 and 2029 and mean annual rainfall under Scenario I (Trend of LULC evolution) is presented in Table 28.

Table 28. Estimation of nitrogen and phosphorus export under Scenario I.

Year	Area	Nitrogen Export		Phosphorus Export		Mean Annual Rainfall
	km ²	Total (kg)	Average (kg/km ²)	Total (kg)	Average (kg/km ²)	(mm)
2020	891.35	197,972.93	222.10	43,358.11	48.64	1523.53
2021	891.35	199,580.02	223.91	43,832.43	49.18	1508.50
2022	891.35	200,858.16	225.34	44,196.29	49.58	1465.20
2023	891.35	202,275.64	226.93	44,619.00	50.06	1517.76
2024	891.35	203,395.90	228.19	44,951.18	50.43	1537.45
2025	891.35	205,172.77	230.18	45,494.30	51.04	1544.38
2026	891.35	206,743.37	231.94	45,966.11	51.57	1486.75
2027	891.35	207,795.18	233.12	46,273.02	51.91	1472.48
2028	891.35	209,325.14	234.84	46,740.48	52.44	1539.43
2029	891.35	210,907.86	236.62	47,221.47	52.98	1498.28

As a result, the highest total and average nitrogen export occurred in 2029, with values of about 210,908 kg and 236.62 kg/km², respectively, while the lowest total and average nitrogen export occurred in 2020 with a value of about 197,973 kg and 222.10 kg/km², respectively. Likewise, the highest total and average phosphorus export occurred in 2029, with a value of about 47,221 kg and 52.98 kg/km², respectively, while the lowest total and average phosphorus export occurred in 2020, of about 43,358 kg and 48.64 kg/km², respectively.

These results indicate that the changes in LULC types and areas affect parameters in the biophysical table, leading to different nitrogen and phosphorus export. In contrast, the annual rainfall, as a runoff proxy, was not observed as being sensitive to the estimated data, due to its calculation to modify the load, in order to account for runoff potential by relating the precipitation per cell to the average over the raster, as suggested by [61]. Therefore, non-linear regression analysis was considered in order to reconfirm the suggestion of [61] and the previous study of [62].

Figure 11 shows the results of non-linear regression analysis between mean annual rainfall (mm) and average nutrient export (kg per km²). The best fit of the non-linear regression by Trend Analysis in the MS Excel software was a sixth-order polynomial equation with R² values of 0.9638 for nitrogen export and 0.9615 for phosphorus export. As a result, it was confirmed that annual rainfall, as a runoff proxy, is not sensitive to the estimated nutrient export under the NDR model.

Furthermore, the contribution of the predicted LULC under Scenario I on nutrient export indicated that the highest total nitrogen and phosphorus export occurred on paddy fields. In contrast, the lowest total nitrogen export occurred on water bodies, and the lowest total phosphorus export occurred on miscellaneous land; however, the highest average nitrogen and phosphorus export appeared on field crops, as well as perennial trees and orchards.

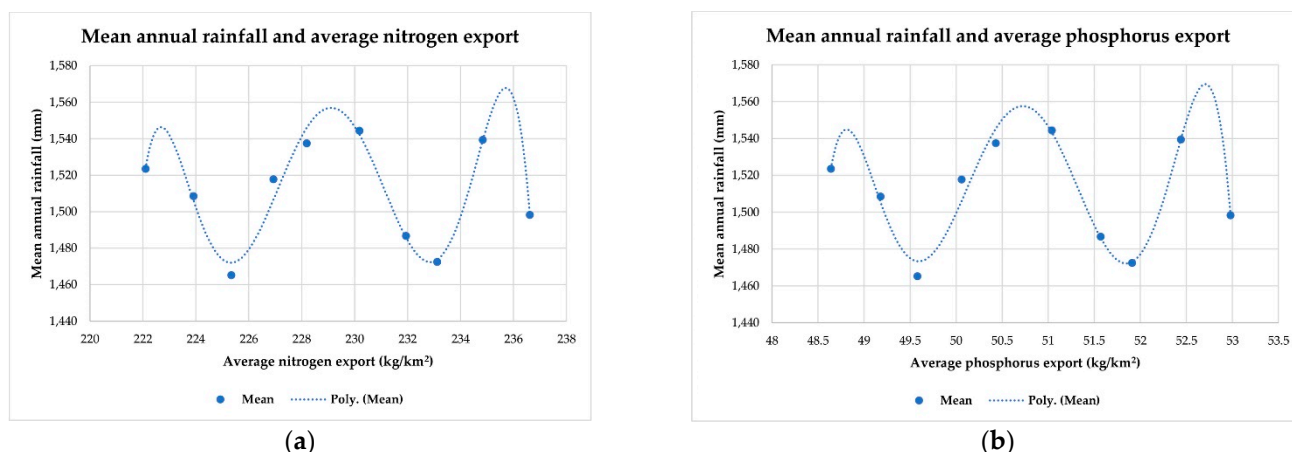


Figure 11. Relationship between mean annual rainfall and average nutrient export under Scenario I: (a) nitrogen and (b) phosphorus.

These findings suggest that the change in LULC types associated with the biophysical table parameters affects nitrogen and phosphorus export. The LULC data of Scenario I were simulated based on the annual rate of LULC change from the transition area matrix between 2009 and 2019 using the Markov Chain model, which did not represent dramatic change under this scenario; the minor change in area also changed the load amounts and export of nutrients.

4.8.3. Nutrient Export Estimation of Predicted LULC under Scenario II

The estimated total and average nitrogen and phosphorus export of predicted LULC between 2020 and 2029 and mean annual rainfall under Scenario II (Maximization of ecosystem service values) is presented in Table 29.

Table 29. Estimation of nitrogen and phosphorus export between 2020 and 2029 under Scenario II.

Year	Area	Nitrogen Export		Phosphorus Export		Mean Annual Rainfall
	km ²	Total (kg)	Average (kg/km ²)	Total (kg)	Average (kg/km ²)	(mm)
2020	891.35	196,964.74	220.97	43,117.85	48.37	1523.53
2021	891.35	195,883.51	219.76	42,988.62	48.23	1508.50
2022	891.35	195,426.12	219.25	42,961.10	48.20	1465.20
2023	891.35	195,754.01	219.62	43,137.70	48.40	1517.76
2024	891.35	195,641.77	219.49	43,160.14	48.42	1537.45
2025	891.35	195,988.64	219.88	43,334.48	48.62	1544.38
2026	891.35	195,915.15	219.80	43,415.07	48.71	1486.75
2027	891.35	196,276.87	220.20	43,540.77	48.85	1472.48
2028	891.35	196,689.44	220.66	43,714.70	49.04	1539.43
2029	891.35	196,815.34	220.81	43,797.81	49.14	1498.28

As a result, the highest total and average nitrogen export occurred in 2020, with values of about 196,965 kg and 220.97 kg/km², respectively, while the lowest total and average nitrogen export occurred in 2022, with values of about 195,426 kg and 219.25 kg/km², respectively. Likewise, the highest total and average phosphorus export were in 2029, with values of about 43,798 kg and 49.14 kg/km², respectively, while the lowest total and average phosphorus export occurred in 2022, with values of about 42,961 kg and 48.20 kg/km², respectively. These results indicate that the changes in LULC types and areas affect parameters in the biophysical table, leading to variations in nitrogen and phosphorus export.

As with Scenario I, the annual rainfall, as a runoff proxy, was not a sensitive factor for estimating nutrients. The best fit of the sixth-order polynomial equation between annual rainfall and nutrient export had R^2 values of 0.4920 for nitrogen export and 0.8834 for phosphorus export (Figure 12).

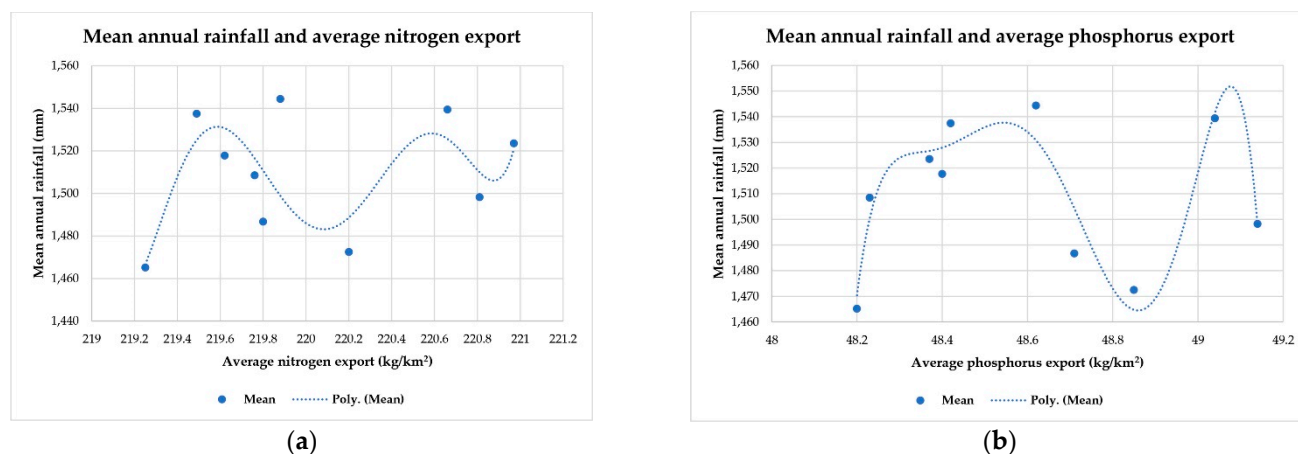


Figure 12. Relationship between mean annual rainfall and average nutrient export under Scenario II: (a) nitrogen and (b) phosphorus.

Moreover, the contribution of the predicted LULC under Scenario II on nutrient export demonstrated that the highest total nitrogen and phosphorus export occurred on the paddy fields. In contrast, the lowest nitrogen export occurred on water bodies, while the lowest phosphorus export occurred on miscellaneous land; however, the highest average nitrogen export appeared on paddy fields and field crops, while the highest average phosphorus export occurred on perennial trees and orchards.

Additionally, these findings suggest that the change in LULC types associated with the biophysical table parameters affects nitrogen and phosphorus export. Notably, the LULC data under this scenario influenced nutrient export due to the LULC data of Scenario II, simulated based on the annual rate of LULC change from transition area matrix between 2009 and 2019 for some LULC types and the LP to maximize ecosystem service values, by reducing the area of rangeland and miscellaneous land and increasing the area of wetland. Therefore, significant LULC change was observed under this scenario, due to the area change, load amounts, and export of nutrients.

4.8.4. Nutrient Export Estimation of Predicted LULC under Scenario III

The estimated total and average nitrogen and phosphorus export according to the predicted LULC between 2020 and 2029 and mean annual rainfall under Scenario III (Economic crop zonation) are presented in Table 30.

As a result, the highest total and average nitrogen export under Scenario III were about 229,756 kg and 257.76 kg/km², respectively, occurring in 2029, while the lowest total and average nitrogen export were about 200,387 kg and 224.81 kg/km², respectively, occurring in 2020. Likewise, the highest total and average phosphorus export were about 51,149 kg and 57.38 tons/km², respectively, occurring in 2029, while the lowest total and average phosphorus export were about 43,956 kg and 49.31 kg/km², respectively, occurring in 2020. These results indicate that the changes in LULC types and areas affect parameters in the biophysical table, which leads to different nitrogen and phosphorus export, as observed in Scenarios I and II. The best fit of the sixth-order polynomial equation between annual rainfall and nutrient export had R^2 values of 0.9530 for nitrogen export and 0.9469 for phosphorus export (Figure 13).

Table 30. Estimation of nitrogen and phosphorus export between 2020 and 2029 under Scenario III.

Year	Area	Nitrogen Export		Phosphorus Export		Mean Annual Rainfall
	km ²	Total (kg)	Average (kg/km ²)	Total (kg)	Average (kg/km ²)	(mm)
2020	891.35	200,387.36	224.81	43,956.03	49.31	1523.53
2021	891.35	204,228.36	229.12	44,919.41	50.39	1508.50
2022	891.35	207,404.15	232.69	45,715.39	51.29	1465.20
2023	891.35	210,923.54	236.63	46,580.29	52.26	1517.76
2024	891.35	213,774.11	239.83	47,267.91	53.03	1537.45
2025	891.35	217,498.34	244.01	48,206.67	54.08	1544.38
2026	891.35	220,573.44	247.46	48,942.83	54.91	1486.75
2027	891.35	223,621.85	250.88	49,650.28	55.70	1472.48
2028	891.35	226,714.19	254.35	50,389.99	56.53	1539.43
2029	891.35	229,756.13	257.76	51,149.42	57.38	1498.28

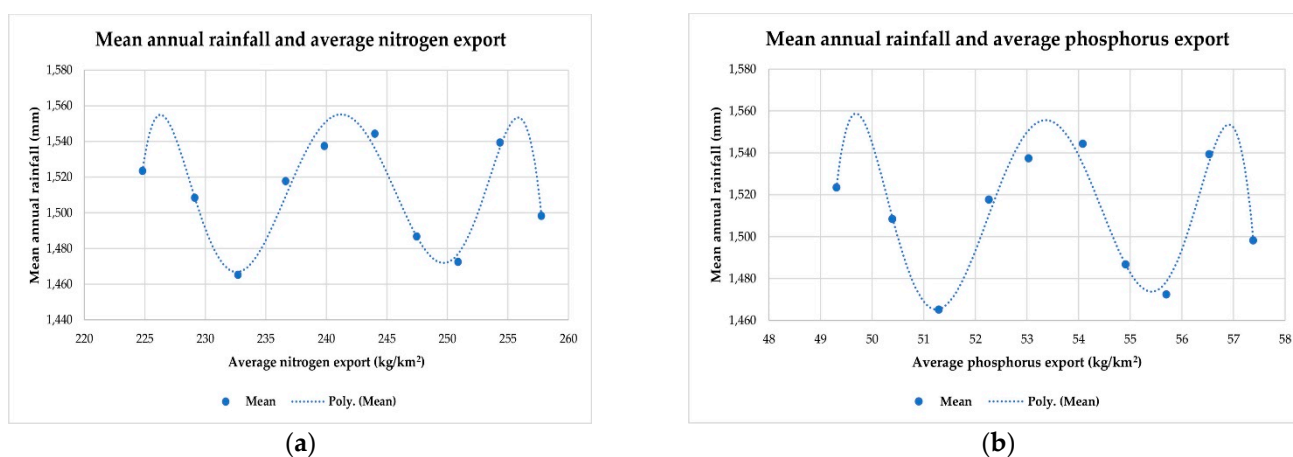


Figure 13. Relationship between mean annual rainfall and average nutrient export under Scenario III: (a) nitrogen and (b) phosphorus.

Furthermore, the contribution of the predicted LULC under Scenario III on nutrient export indicated that the highest total nutrient and phosphorus export occurred on paddy fields. In contrast, the lowest total nitrogen export occurred on water bodies, while the lowest total phosphorus export occurred on miscellaneous land. Meanwhile, the highest average nitrogen and phosphorus export occurred on field crops, as well as perennial trees and orchards.

These findings suggest that the change in LULC types associated with the biophysical table parameters affects nitrogen and phosphorus export. In particular, the LULC data under this scenario influenced nutrient export, according to the LULC data of Scenario III simulated based on the annual rate of LULC change from transition area matrix between 2009 and 2019 for some LULC types and the economic crop zonation, particularly the increase in paddy field and field crop areas and the decrease in perennial tree and orchard areas, which represented dramatic change under this scenario, leading to changes in the load amounts and export of nutrients. Hence, significant LULC change was observed under this scenario.

The average nutrient (N and P) export between 2020 and 2029 for the three scenarios was compared, as shown in Figure 14, which shows that the predicted LULC under Scenario II (Maximization of ecosystem service values) delivered the lowest annual nitrogen and phosphorus export, compared to Scenarios I and III, due to the allocation of area using LP to maximize the ecosystem service values by increasing wetland areas. Increases in wetland areas, such as wetland restoration and constructed riparian wetlands, can reduce nitrogen [63] and phosphorus [64] export into water bodies. Furthermore, based

on the biophysical table, wetland provides the highest maximum retention efficiency and provides low nitrogen and phosphorus load. The decreased paddy field area under scenario II affected the nutrient export, as this LULC type supplies the highest nitrogen and phosphorus load with low maximum retention efficiency.

Nevertheless, scenario III (Economic crop zonation) generated higher nutrient export than other scenarios, as the paddy field and field crop areas were increased according to their LDD suitability classes. These areas provide the highest nitrogen and phosphorus load, but low maximum retention efficiency. This result is in agreement with [65], who applied the NDR model to calculate nutrient export under two different scenarios. They found that the cropland balance policy negatively impacted water purification by increasing nitrogen export, which was 8.36% higher than that in the no strict cropland protection scenario.

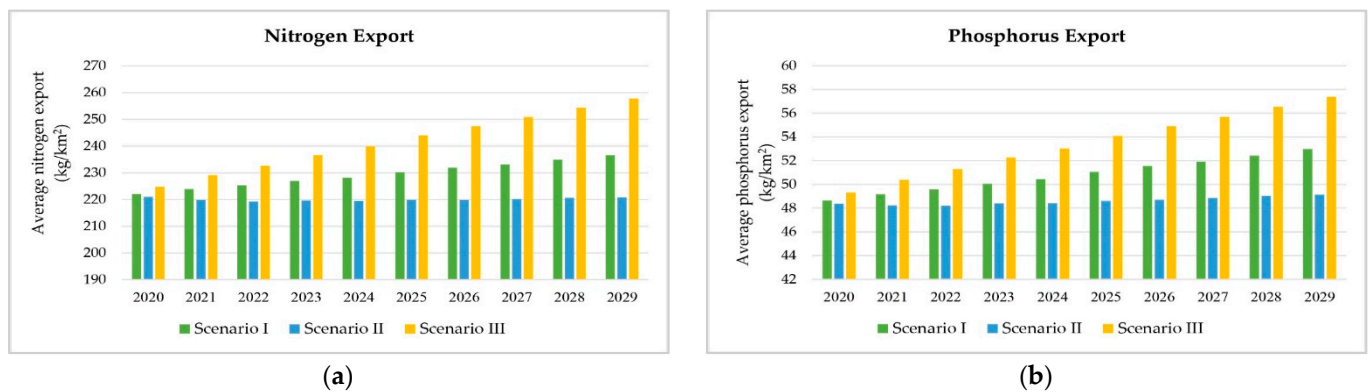


Figure 14. Comparison of nutrient export between 2020 and 2029 of three scenarios: (a) nitrogen and (b) phosphorus.

4.9. Suitable LULC Allocation Scenario to Minimize Sediment Export

The ESCI values of sediment export in ten periods—as well as its average under the three scenarios—were compared, in order to identify a suitable LULC allocation scenario for minimizing sediment export, in terms of ecosystem service change, as summarized in Table 31 and Figure 15.

Table 31. Sediment export and ESCI value and its average under three different scenarios.

Year	Period	Scenario I		Scenario II		Scenario III	
		Sediment Export (tons)	ESCI	Sediment Export (tons)	ESCI	Sediment Export (tons)	ESCI
2019		26,421.41		26,421.41		26,421.41	
2020	2019–2020	41,445.02	0.5686	40,979.13	0.5510	43,130.50	0.6324
2021	2019–2021	35,685.45	0.3506	34,149.06	0.2925	37,330.55	0.4129
2022	2019–2022	32,373.49	0.2253	30,190.61	0.1427	34,520.48	0.3065
2023	2019–2023	41,954.52	0.5879	38,483.96	0.4565	46,451.16	0.7581
2024	2019–2024	39,669.68	0.5014	35,659.13	0.3496	47,447.38	0.7958
2025	2019–2025	48,329.18	0.8292	41,526.64	0.5717	59,526.42	1.2530
2026	2019–2026	58,797.97	1.2254	48,115.01	0.8211	76,068.33	1.8790
2027	2019–2027	42,549.03	0.6104	33,851.75	0.2812	59,092.34	1.2365
2028	2019–2028	46,867.05	0.7738	36,216.79	0.3707	67,376.26	1.5501
2029	2019–2029	49,558.85	0.8757	37,599.82	0.4231	74,740.75	1.8288
	Average	43,723.02 *	0.6548	37,677.19 *	0.4260	54,568.42 *	1.0653

Note: * The average value from data between 2020 and 2029.

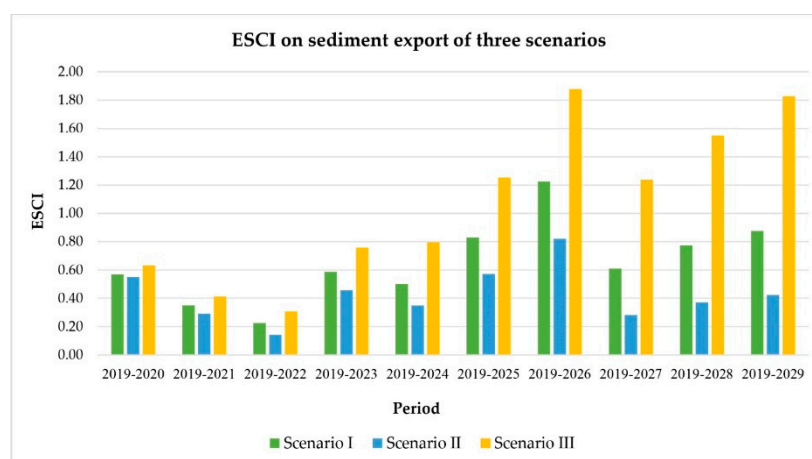


Figure 15. Comparison of ESCI on sediment export in ten periods under three scenarios.

According to the result, the LULC allocation of Scenario II (Maximization of ecosystem service values) generated the lowest sediment export every year between 2020 and 2029, with an average sediment export of 37,677.19 tons. The cumulative ESCI values on sediment export of this scenario were also the lowest, with an average ESCI value of 0.04260. Therefore, the LULC allocation of Scenario II was chosen, in order to minimize the sediment export into Kwan Phayao from the Upper Ing watershed.

Moreover, the average ESCI for sediment export under the three allocation LULC scenarios was tested, in terms of the difference of the mean, using the *t*-test statistic. The results demonstrated significant differences among average ESCI values on sediment export of three scenarios at the 95% confidence level. See detail in Table A8 in Appendix B.

4.10. Suitable LULC Allocation Scenario to Minimize Nutrient Export

The ESCI values for nutrient (N and P) export in ten periods and its average of three scenarios were compared, in order to identify a suitable LULC allocation scenario for minimizing nutrient export, in terms of ecosystem service change, are reported in Tables 32 and 33 and shown in Figures 16 and 17.

Table 32. Nitrogen export and ESCI value and its average of three scenarios.

Year	Period	Scenario I		Scenario II		Scenario III	
		Nitrogen Export (kg)	ESCI	Nitrogen Export (kg)	ESCI	Nitrogen Export (kg)	ESCI
2019		193,307.56		193,307.56		193,307.56	
2020	2019–2020	197,972.93	0.0241	196,964.74	0.0189	200,387.36	0.0366
2021	2019–2021	199,580.02	0.0324	195,883.51	0.0133	204,228.36	0.0565
2022	2019–2022	200,858.16	0.0391	195,426.12	0.0110	207,404.15	0.0729
2023	2019–2023	202,275.64	0.0464	195,754.01	0.0127	210,923.54	0.0911
2024	2019–2024	203,395.90	0.0522	195,641.77	0.0121	213,774.11	0.1059
2025	2019–2025	205,172.77	0.0614	195,988.64	0.0139	217,498.34	0.1251
2026	2019–2026	206,743.37	0.0695	195,915.15	0.0135	220,573.44	0.1410
2027	2019–2027	207,795.18	0.0749	196,276.87	0.0154	223,621.85	0.1568
2028	2019–2028	209,325.14	0.0829	196,689.44	0.0175	226,714.19	0.1728
2029	2019–2029	210,907.86	0.0910	196,815.34	0.0181	229,756.13	0.1886
	Average	204,402.70 *	0.0574	196,135.56 *	0.0146	215,488.15 *	0.1147

Note: * The average value from data between 2020 and 2029.

Table 33. Phosphorus export and ESCI value and its average of three scenarios.

Year	Period	Scenario I		Scenario II		Scenario III	
		Phosphorus Export (kg)	ESCI	Phosphorus Export (kg)	ESCI	Phosphorus Export (kg)	ESCI
2019		41,978.66		41,978.66		41,978.66	
2020	2019–2020	43,358.11	0.0329	43,117.85	0.0271	43,956.03	0.0471
2021	2019–2021	43,832.43	0.0442	42,988.62	0.0241	44,919.41	0.0701
2022	2019–2022	44,196.29	0.0528	42,961.10	0.0234	45,715.39	0.0890
2023	2019–2023	44,619.00	0.0629	43,137.70	0.0276	46,580.29	0.1096
2024	2019–2024	44,951.18	0.0708	43,160.14	0.0281	47,267.91	0.1260
2025	2019–2025	45,494.30	0.0837	43,334.48	0.0323	48,206.67	0.1484
2026	2019–2026	45,966.11	0.0950	43,415.07	0.0342	48,942.83	0.1659
2027	2019–2027	46,273.02	0.1023	43,540.77	0.0372	49,650.28	0.1828
2028	2019–2028	46,740.48	0.1134	43,714.70	0.0414	50,389.99	0.2004
2029	2019–2029	47,221.47	0.1249	43,797.81	0.0433	51,149.42	0.2185
Average		45,265.24 *	0.0783	43,316.82 *	0.0319	47,677.82 *	0.1358

Note: * The average value from data between 2020 and 2029.

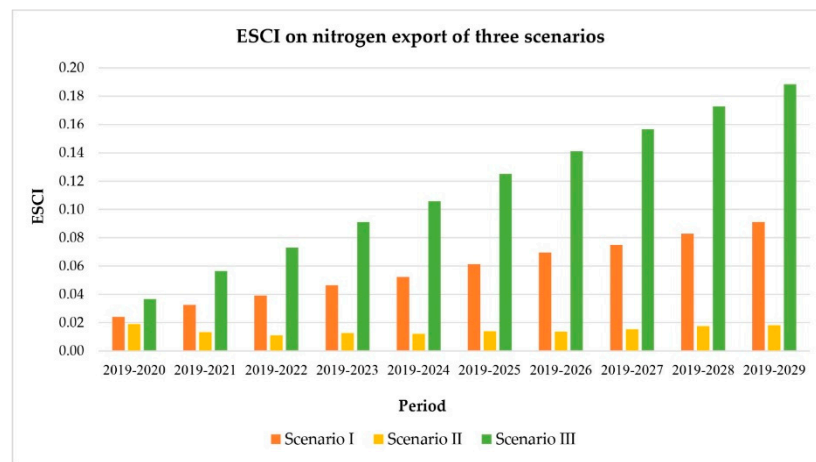


Figure 16. Comparison of ESCI on nitrogen export of three scenarios in 10 periods.

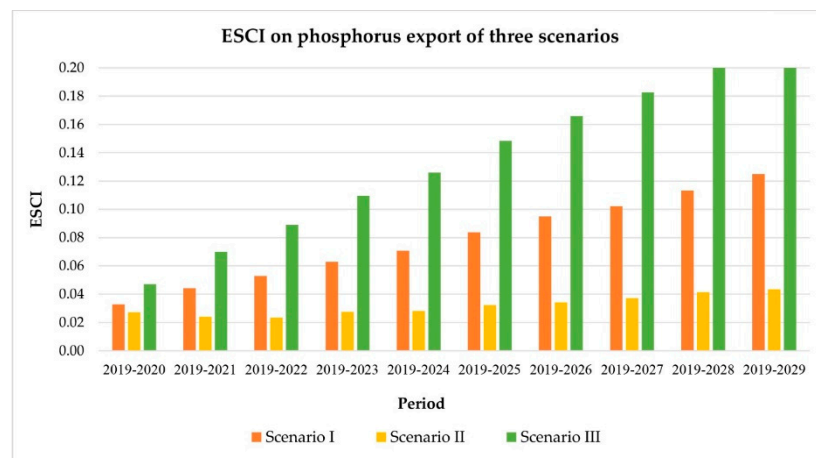


Figure 17. Comparison of ESCI on phosphorus export of three scenarios in 10 periods.

As a result, Scenario II (Maximization of ecosystem service values) produced the lowest nutrient (N and P) export every year between 2020 and 2029, with average values of 196,135.56 kg for nitrogen and 43,316.82 kg for phosphorus. The cumulative ESCI values for nutrient export under this scenario were also the lowest, with average ESCI

values for nitrogen of 0.0146 and phosphorus of 0.0319. Therefore, the LULC allocation under Scenario II was selected to minimize nutrient export into Kwan Phayao, the Upper Ing watershed.

Moreover, the average ESCI on nitrogen and phosphorus export of three LULC allocation scenarios was used to test the mean differences using the *t*-test statistic. The results revealed significant differences among average ESCI values for nutrient export under the three scenarios at the 95% confidence level. See detail in Tables A9 and A10 in Appendix B.

4.11. Suitable LULC Allocation Scenario to Minimize Sediment and Nutrient Export

The average ESCI values for sediment and nutrient (N and P) exports in ten periods of three LULC allocation scenarios were compared, in order to identify suitable LULC allocation scenarios to minimize sediment and nutrient export, in terms of ecosystem service change, as shown in Figure 18 and summarized in Table 34.

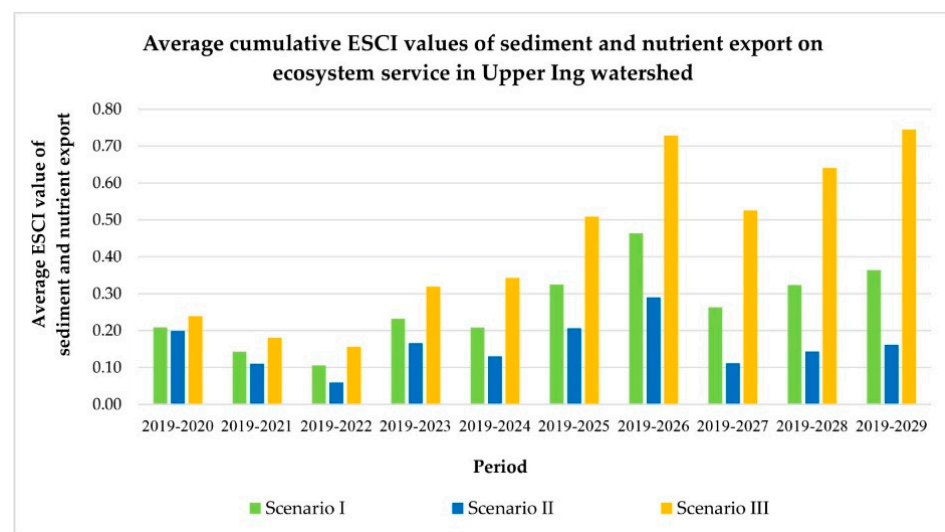


Figure 18. Comparison of average ESCI value of sediment and nutrient export on ecosystem services among the three scenarios.

Table 34. Average ESCI values of sediment and nutrient export on ecosystem service among the three considered scenarios.

Period	Scenario I				Scenario II				Scenario III			
	Sediment	N	P	Avg.	Sediment	N	P	Avg.	Sediment	N	P	Avg.
2019–2020	0.5686	0.0241	0.0329	0.2085	0.5510	0.0189	0.0271	0.1990	0.6324	0.0366	0.0471	0.2387
2019–2021	0.3506	0.0324	0.0442	0.1424	0.2925	0.0133	0.0241	0.1100	0.4129	0.0565	0.0701	0.1798
2019–2022	0.2253	0.0391	0.0528	0.1057	0.1427	0.0110	0.0234	0.0590	0.3065	0.0729	0.0890	0.1562
2019–2023	0.5879	0.0464	0.0629	0.2324	0.4565	0.0127	0.0276	0.1656	0.7581	0.0911	0.1096	0.3196
2019–2024	0.5014	0.0522	0.0708	0.2081	0.3496	0.0121	0.0281	0.1299	0.7958	0.1059	0.1260	0.3426
2019–2025	0.8292	0.0614	0.0837	0.3248	0.5717	0.0139	0.0323	0.2060	1.2530	0.1251	0.1484	0.5088
2019–2026	1.2254	0.0695	0.0950	0.4633	0.8211	0.0135	0.0342	0.2896	1.8790	0.1410	0.1659	0.7287
2019–2027	0.6104	0.0749	0.1023	0.2625	0.2812	0.0154	0.0372	0.1113	1.2365	0.1568	0.1828	0.5254
2019–2028	0.7738	0.0829	0.1134	0.3234	0.3707	0.0175	0.0414	0.1432	1.5501	0.1728	0.2004	0.6411
2019–2029	0.8757	0.0910	0.1249	0.3639	0.4231	0.0181	0.0433	0.1615	1.8288	0.1886	0.2185	0.7453
Average				0.2635				0.1575				0.4386

As a result, the average cumulative ESCI values for sediment and nutrient export ecosystem services under the LULC allocation of Scenario II (Maximization of ecosystem service values) provided the lowest value, with an average ESCI value of 0.1575 among different LULC scenarios. Additionally, Scenario II created the lowest yield of sediment, nitrogen, and phosphorus exports between 2000 and 2029 among the scenarios, with average values of about 37,678 tons, 196,136 kg, and 43,317 kg, respectively.

Therefore, the LULC allocation of Scenario II (Maximization of ecosystem service values) was selected as the suitable LULC allocation scenario to minimize sediment and nutrient exports into Kwan Phayao from the Upper Ing watershed. These findings can serve as crucial information to allocate LULC in the Upper Ing watershed by land-use planners, land managers, and decision-makers in order to minimize sediment and nutrient loads into Kwan Phayao in the future.

5. Discussion

5.1. LULC Classification Using SVM Algorithm

The overall accuracy and Kappa hat coefficient for the thematic accuracy of the LULC map in 2009 and 2019 were 90.86 and 87.00%, and 89.59 and 85.85%, respectively. Kappa hat coefficient values of more than 80% represent a substantial agreement between the classification map and the reference data [66]; likewise, the overall accuracy of the LULC maps—higher than 85%—indicates that they can provide an acceptable result [67].

In addition, the overall accuracy and Kappa hat coefficient of the current study were consistent with other researchers who have classified LULC data based on Landsat imagery using the SVM algorithm [68–71]; however, to apply SVM for LULC classification, users must select sample points between the boundaries of LULC classes precisely, where mixed pixels are common, in order to ensure accurate classification [72]. Therefore, selecting the SVM algorithm's training points for LULC classification under the EnMap BOX software requires time and skill.

5.2. Land Requirement Estimation under Three Different Scenarios

Land requirement is essential information for LULC prediction using the CLUE-S model. In this study, three different scenarios including (1) Scenario I (Trend of LULC evolution), (2) Scenario II (Maximization of ecosystem service values), and Scenario III (Economic crop zonation) are estimated based on their characteristics. The land requirement of Scenario I is estimated based on the annual change rate of LULC between 2009 and 2019 from the transition area matrix using the Markov Chain model. The land requirement of Scenario I is dictated by the accuracy of LULC data in 2009 and 2019. Meanwhile, the land requirement of Scenario II is estimated based on LULC allocation for maximizing ESV using Linear Programming with the Simplex method. The land requirement of Scenario II depends on the efficiency of linear programming for determining reclaimed and other areas changing into the wetland. At the same time, the land requirement of Scenario III is estimated based on areas of suitability classes for economic crops (paddy field, field crop, para rubber, and perennial trees and orchards) and the Markov Chain model. The land requirement of Scenario III is delimited by the economic crop zonation and the accuracy of LULC data in 2019. Consequently, the definition of each Scenario should first be well defined and local government agencies and stakeholders should be consulted before land requirement estimation.

5.3. LULC Prediction by CLUE-S Model

According to binary logistics regression analysis, the derived AUC values for each LULC type allocation under the CLUE-S model exhibit good fit (0.80) and excellent fit (0.99) between the predicted and real LULC transition, as mentioned by Chen et al. [73]. These results imply that the significant driving factors on LULC change, including soil drainage, distance to stream, distance to water body, distance to village, slope, distance to road, annual rainfall, elevation, and population density at subdistrict level, are suitable to apply for each LULC type allocation under CLUE-S model.

As a result of LULC prediction under three scenarios by the CLUE-S model, the predicted LULC data of three scenarios can deliver realistic results as an expectation. The deviation values between the required land area and the predicted area of each LULC type under three scenarios are very small and vary from -0.0023 to 0.0033% or -0.23 km^2 (underestimation) to 0.33 km^2 (overestimation). In principle, the deviation value depends on iteration driving factors of each LULC type, which indicate the maximum different allowance between the land requirement and land allocation of LULC type under the CLUE-S model [53,54].

Consequently, the CLUE-S model can be an effective tool to predict LULC data according to specific policies as the scenario. Essentially, the suitable multiple linear equations from the logistics regression analysis for each LULC type allocation, a land requirement of different scenarios assigned by policy transformation, and model parameters (elasticity and LULC conversion matrix) are very important for predicting LULC under the CLUE-S model.

5.4. Sediment Export Estimation

According to the results of sediment export estimation, it was found that the primary influence of rainfall erosivity and LULC types in the RUSLE model affect sediment export under three different scenarios. The rainfall erosivity can explain the linear relationship with the sediment export from about 27% in Scenario III (Economic crop zonation) to 96% in Scenario II (Maximization of ecosystem service values). These findings are consistent with the previous studies [56–60].

The contribution of the predicted LULC under three scenarios on sediment export between 2020 and 2029 indicated that miscellaneous land causes the highest average sediment export. Meanwhile, forest land generates the lowest average sediment export. This finding was consistent with the previous study of Srichaichana et al. [14]. They found that miscellaneous land (bare land and abandoned mine) created the highest average sediment export, with a value of 659.72 tons/km^2 . At the same time, evergreen forest generated the lowest average sediment export, with a value of 0.01 tons/km^2 , in the Klong U-Tapao watershed, Songkhla Province, Thailand. Likewise, Degife et al. [74] found that the highest sediment export per unit of area was observed from miscellaneous land (bare land), while the highest contribution of the total sediment that reached the surrounding water bodies was from cultivated land (40.7%). Similarly, Zhou et al. [75] found that decreases in miscellaneous land (bare land) significantly reduced sediment export in the Qiantang River Basin, China. In contrast, increases in agricultural land, such as cropland and garden plots, increased sediment export in the studied watershed.

5.5. Nutrient Export Estimation

The nutrient (N and P) export estimation under three different scenarios indicates that the change in LULC types and areas affects parameters in the biophysical table, leading to different nitrogen and phosphorus export. The contribution of LULC type under three scenarios indicates that the highest total nitrogen and phosphorus exports occur on paddy fields. In contrast, the lowest total nitrogen export occurs on water bodies, and the lowest total phosphorus export occurs on miscellaneous land. However, the highest average nitrogen and phosphorus export mostly appeared on field crops and perennial trees/orchards. These findings agree with [76], who indicated that the highest nitrogen and phosphorus exports occurred on cultivated land. There was very little nitrogen and phosphorus export on forest land, water areas, and unused land. This is similar to the result of [77], who analyzed nutrient load and delivery from different scenarios and found the most significant load rate per unit area and low retention efficiency of cultivated crops. Furthermore, agriculture was the leading cause of nutrient release in the watershed under the different LULC scenarios. These findings are similar to those of [78], who found that cropland and agroforestry influenced roughly 90% of the nutrients exported, while water bodies were identified as sinks.

Moreover, as a runoff proxy, the annual rainfall is not a sensitive factor for estimating nutrients, as suggested by [61] and the previous study of [62]. The best fit of the sixth-order polynomial equation between annual rainfall and nutrient (N and P) export under three different scenarios in this study reconfirm the relationship as mentioned earlier. In this study, the R^2 value of the relations between annual rainfall and nitrogen export varies from 0.4920 to 0.9638, while the R^2 value of the relations between annual rainfall and phosphorus export diverges from 0.8834 to 0.9615.

6. Conclusions

Land-use and land-cover (LULC) classification and change detection between 2009 and 2019 was successfully conducted using a supervised classification with a support vector machine and post-classification comparison change detection algorithms. The overall accuracy and Kappa hat coefficient of the LULC maps in 2009 and 2019 were higher than 85%. Then, the land requirements under three scenarios—Scenario I (Trend of LULC evolution), Scenario II (Maximization of ecosystem service values), and Scenario III (Economic crop zonation)—were estimated based on their characteristics. Time-series LULC data between 2020 and 2029 were then effectively predicted using the CLUE-S model. After that, the actual LULC data in 2019, as base data, and the predicted LULC data under the three scenarios between 2020 and 2029 were used as significant inputs for ecosystem service assessment, in terms of sediment and nutrient export, using the SDR and NDR models. Finally, a suitable LULC allocation scenario was successfully identified in order to minimize sediment and nutrient export using the ecosystem services change index: the most suitable LULC allocation scenario to minimize sediment or/and nutrient export into Kwan Phayao was Scenario II (Maximization of ecosystem service value).

In conclusion, the integration of remote sensing data with an advanced classification method (support vector machine classifier), GIS data with linear programming, and advanced geospatial models (CLUE-S model, SDR and NDR model) can be used as an efficient tool to assess ecosystem services at the watershed level—particularly sediment and nutrient (N and P) export—and can be further applied to identify a suitable LULC allocation scenario to minimize sediment and nutrient export into certain lakes. The results of the current study can serve as crucial information for land-use planners, land managers, and decision-makers in order to reduce sediment and nutrient export into Kwan Phayao in the future.

Author Contributions: Conceptualization, S.O. and J.K.; methodology, S.O. and J.K.; software, J.K.; validation, S.O. and J.K.; formal analysis, S.O. and J.K.; investigation, S.O. and J.K.; data curation, J.K.; writing—original draft preparation, J.K.; writing—review and editing, S.O.; visualization, J.K.; supervision, S.O. All authors have read and agreed to the published version of the manuscript.

Funding: This research received no external funding.

Institutional Review Board Statement: Not applicable.

Informed Consent Statement: Not applicable.

Data Availability Statement: Not applicable.

Acknowledgments: The authors would like to thank the Suranaree University of Technology for providing a scholarship to Jiraporn Kulsoontornrat and the University of Phayao for supporting the facilities to undertake this research. Special thanks from the authors go to the anonymous reviewers for their valuable comments and suggestions that improved our manuscript from various perspectives.

Conflicts of Interest: The authors declare no conflict of interest.

Appendix A

Table A1. Soil series and geology unit sand soil erodibility factor values.

Soil Series	Erodibility Factor Value	Slope Complex	
		Geology Units	Erodibility Factor Value
Chaing Rai series	0.27	Jurassic (J)	0.15
Hang Chat series	0.27	Jurassic–Cretaceous (JK)	0.27
Hang Chat/Renu association	0.27	Cretaceous (K)	0.27
Hang Dong series	0.18	Permian (P)	0.15
Lampang series	0.34	Quaternary Alluvium (Qa)	0.19
Mae Rim/Hang Chat Association	0.27	Quaternary (Qc)	0.27
Mae Sai series	0.27	Pleistocene (Qt)	0.27
Nan series	0.27	Triassic (Trhh)	0.27
Phan series	0.18	Igneous rock	0.30
Phayao series	0.18		
Phimai series	0.18		
Pran Buri, mottle Variant	0.27		
Tha Muang/Sanphaya Association	0.27		
Tha Yang/Lat Ya Association	0.27		

Source: [22].

Table A2. Values of the C and P factors corresponding to each LULC type.

No	LULC Type	C Factor of RUSLE	P Factor of RUSLE
1	Urban and built-up area	0.000	0.000
2	Paddy field	0.280	0.100
3	Field crop	0.340	1.000
4	Para rubber	0.150	1.000
5	Perennial trees and orchards	0.150	1.000
6	Forest land	0.001	1.000
7	Water body	0.000	0.000
8	Rangeland	0.032	1.000
9	Wetland	0.000	0.000
10	Miscellaneous land	0.800	1.000

Source: [22].

Appendix B

Table A3. Multicollinearity test for effect of driving factors on LULC type.

No.	Driving Factor	Unstandardized Coefficients		Standardized Coefficient	t-Test	Sig.	VIF
		Beta	Std. Error				
1	Soil drainage (X_1)	−0.0229	0.0056	−0.0207	−4.1086	0.0000	1.4736
2	Distance to stream (X_2)	0.0011	0.0000	0.1476	33.5946	0.0000	1.1226
3	Distance to water body (X_3)	−0.0002	0.0000	−0.3006	−29.9464	0.0000	5.8550
4	Distance to village (X_4)	0.0003	0.0000	0.3579	66.7967	0.0000	1.6688
5	Slope (X_5)	0.0142	0.0008	0.1225	17.8190	0.0000	2.7464
6	Distance to road (X_6)	0.0003	0.0000	0.2327	26.3178	0.0000	4.5438
7	Distance to fault line (X_7)	−0.0001	0.0000	−0.0991	−18.5922	0.0000	1.6527
8	Annual rainfall (X_8)	0.0015	0.0001	0.0737	12.3901	0.0000	2.0576
9	Elevation (X_9)	0.0011	0.0001	0.0966	12.5618	0.0000	3.4356
10	Income per capita at subdistrict level (X_{10})	0.0000	0.0000	0.0271	3.1387	0.0017	4.3486
11	Population density at subdistrict level (X_{11})	−0.0005	0.0001	−0.0576	−7.0590	0.0000	3.8632

Table A4. Deviation between estimated land requirements and predicted LULC data in 2029 under Scenario I.

Item	LULC Type										Total
	UR	PD	FC	RB	PO	FO	WB	RL	WL	ML	
Predicted LULC 2029	36.90	210.84	22.81	28.45	98.75	400.39	41.35	33.36	14.82	3.68	891.35
Land requirement 2029	36.92	210.86	22.79	28.45	98.74	400.38	41.34	33.36	14.80	3.70	891.35
Deviation value (%)	−0.0002	−0.0002	0.0002	0.00	0.0001	0.0001	0.0001	0.00	0.0002	−0.0002	0.00
Deviation value (km ²)	−0.02	−0.02	0.02	0.00	0.01	0.01	0.01	0.00	0.02	−0.02	0.00

Table A5. Constraints set to maximize ecosystem service values under Scenario II.

Constraints	UR	PD	FC	RP	PO	FO	WB	RL	WL	ML	Operator	Area (ha)	Remark
	(X1)	(X2)	(X3)	(X4)	(X5)	(X6)	(X7)	(X8)	(X9)	(X10)			
Constraint 1	1	1	1	1	1	1	1	1	1	1	=	89,135.00	Total area
Constraint 2 (UR)	1	0	0	0	0	0	0	0	0	0	=	3692.29	MCM
Constraint 3 (PD)	0	1	0	0	0	0	0	0	0	0	≤	22,074.23	LULC 2019
Constraint 4 (PD)	0	1	0	0	0	0	0	0	0	0	≥	21,086.41	MCM
Constraint 5 (FC)	0	0	1	0	0	0	0	0	0	0	≤	2279.25	MCM
Constraint 6 (FC)	0	0	1	0	0	0	0	0	0	0	≥	2184.17	LULC 2019
Constraint 7 (RP)	0	0	0	1	0	0	0	0	0	0	≤	2844.72	MCM
Constraint 8 (RP)	0	0	0	1	0	0	0	0	0	0	≥	1978.41	LULC 2019
Constraint 9 (PO)	0	0	0	0	1	0	0	0	0	0	≤	9874.03	MCM
Constraint 10 (PO)	0	0	0	0	1	0	0	0	0	0	≥	7922.37	LULC 2019
Constraint 11 (FO)	0	0	0	0	0	1	0	0	0	0	≤	43,691.43	MCM
Constraint 12 (FO)	0	0	0	0	0	1	0	0	0	0	≥	40,038.00	MCM
Constraint 13 (WB)	0	0	0	0	0	0	1	0	0	0	=	3336.76	LULC 2019
Constraint 14 (RL)	0	0	0	0	0	0	0	1	0	0	≤	2726.21	LULC 2019
Constraint 15 (RL)	0	0	0	0	0	0	0	1	0	0	≥	1363.11	Decreased
Constraint 16 (WL)	0	0	0	0	0	0	0	0	1	0	≤	2985.48	Increased
Constraint 17 (WL)	0	0	0	0	0	0	0	0	1	0	≥	1640.63	LULC 2019
Constraint 18 (ML)	0	0	0	0	0	0	0	0	0	1	≤	271.27	LULC 2019
Constraint 19 (ML)	0	0	0	0	0	0	0	0	0	1	≥	135.64	Decreased

Remark: MCM, Markov Chain Model; LULC 2019, classified LULC in 2019; Decreased, decreased by 50% from LULC 2019; Increased, increased by the reclaimed areas and other LULC types.

Table A6. Deviation of estimated land requirements and predicted LULC data in 2029 under Scenario II.

Item	LULC Type										Total
	UR	PD	FC	RB	PO	FO	WB	RL	WL	ML	
Predicted LULC 2029	36.94	210.78	21.80	28.46	98.68	416.34	33.70	13.57	29.72	1.36	891.35
Land requirement 2029	36.92	210.86	21.84	28.45	98.74	416.32	33.37	13.63	29.85	1.36	891.35
Deviation value (%)	0.0002	−0.0008	−0.0004	0.0001	−0.0006	0.0002	0.0033	−0.0006	−0.0013	0.00	0.00
Deviation value (km ²)	0.02	−0.08	−0.04	0.01	−0.06	0.02	0.33	−0.06	−0.13	0.00	0.00

Table A7. Deviation of estimated land requirements and predicted LULC data in 2029 under Scenario III.

Item	LULC Type										Total
	UR	PD	FC	RB	PO	FO	WB	RL	WL	ML	
Predicted LULC 2029	36.96	280.20	34.11	19.78	26.94	400.22	41.11	33.44	14.85	3.73	891.35
Land requirement 2029	36.92	280.34	33.96	19.66	26.88	400.38	41.34	33.36	14.80	3.70	891.35
Deviation value (%)	0.0004	−0.0014	0.0015	0.0012	0.0006	−0.0016	−0.0023	0.0008	0.0005	0.00	0.00
Deviation value (km ²)	0.04	−0.14	0.15	0.12	0.06	−0.16	−0.23	0.08	0.05	0.03	0.00

Table A8. Results of *t*-test for average ESCI values on sediment export among three scenarios.

Pairwise of Scenario	Mean		Variance		df	t-Stat	t Critical 2-Tail
	Variable 1	Variable 2	Variable 1	Variable 2			
I and II	0.6548	0.4260	0.0815	0.0358	9	4.5002	2.2622
I and III	0.6548	1.0653	0.0815	0.3223	9	−3.9847	2.2622
II and III	0.4260	1.0653	0.0358	0.3223	9	−4.1715	2.2622

Table A9. Results of *t*-test for average ESCI values on nitrogen export among three scenarios.

Pairwise of Scenario	Mean		Variance		df	t-Stat	t Critical 2-Tail
	Variable 1	Variable 2	Variable 1	Variable 2			
I and II	0.0574	0.0146	0.0005	0.0000	9	6.2809	2.2622
I and III	0.0574	0.1147	0.0005	0.0026	9	−6.3392	2.2622
II and III	0.0146	0.1147	0.0000	0.0026	9	−6.3214	2.2622

Table A10. Results of *t*-test for average ESCI values on phosphorus export among three scenarios.

Pairwise of Scenario	Mean		Variance		df	t-Stat	t Critical 2-Tail
	Variable 1	Variable 2	Variable 1	Variable 2			
I and II	0.0783	0.0319	0.0009	0.0000	9	6.0779	2.2622
I and III	0.0783	0.1358	0.0009	0.0033	9	−6.8310	2.2622
II and III	0.0319	0.1358	0.0000	0.0033	9	−6.4782	2.2622

References

- Mushtaq, F.; Pandey, A.C. Assessment of land use/land cover dynamics vis-à-vis hydrometeorological variability in Wular Lake environs Kashmir Valley, India using multitemporal satellite data. *Arab. J. Geosci.* **2013**, *2014*, 4707–4715. [[CrossRef](#)]
- Ballatore, T.J.; Muhandiki, V.S. The case for a World Lake Vision. *Processes* **2002**, *16*, 2079–2089. [[CrossRef](#)]
- ILEC. *Managing Lakes and Their Basin for Sustainable Use: A Report for Lake Basin Managers and Stakeholders*; International Lake Environment Committee Foundation: Kusatsu, Japan, 2005.
- Huang, J.; Zhan, J.; Yan, H.; Wu, F.; Deng, X. Evaluation of the Impacts of Land Use on Water Quality: A Case Study in The Chaohu Lake Basin. *Sci. World J.* **2013**, *2013*, 329187. [[CrossRef](#)] [[PubMed](#)]
- Hua, A.K. Land Use Land Cover Changes in Detection of Water Quality: A Study Based on Remote Sensing and Multivariate Statistics. *J. Environ. Public Health* **2017**, *2017*, 7515130. [[CrossRef](#)] [[PubMed](#)]
- Heathcote, A.J.; Filstrup, C.T.; Downing, J.A. Watershed Sediment Losses to Lakes Accelerating Despite Agricultural Soil Conservation Efforts. *PLoS ONE* **2013**, *8*, e53554. [[CrossRef](#)] [[PubMed](#)]
- Fu, B.; Zhang, L.; Xu, Z.; Zhao, Y.; Wei, Y.; Skinner, D. Ecosystem services in changing land use. *J. Soils Sediments* **2015**, *15*, 833–843. [[CrossRef](#)]
- Alcamo, J.; Bennett, E.M. *Ecosystems and Human Well-Being: A Framework for Assessment*; Island Press: Washington, DC, USA, 2003.
- Millennium Ecosystem Assessment (Program). *Ecosystems and Human Well-Being*; Island Press: Washington, DC, USA, 2005.

10. Veldkamp, A.; Verburg, P.H. Editorial, Modelling land use change and environmental impact. *J. Environ. Manag.* **2004**, *72*, 1–3. [[CrossRef](#)]
11. Yuan, F. Land-cover change and environmental impact analysis in the Greater Mankato area of Minnesota using remote sensing and GIS modelling. *Int. J. Remote Sens.* **2008**, *29*, 1169–1184. [[CrossRef](#)]
12. Tolessa, T.; Senbeta, F.; Kidane, M. The impact of land use/land cover change on ecosystem services in the central highlands of Ethiopia. *Ecosyst. Serv.* **2017**, *23*, 47–54. [[CrossRef](#)]
13. Shoyamaa, K.; Kamiyamaa, C.; Morimotob, J.; Oobac, M.; Okurod, T. A review of modeling approaches for ecosystem services assessment in the Asian region. *Ecosyst. Serv.* **2017**, *26*, 316–328. [[CrossRef](#)]
14. Srichaichana, J.; Trisurat, Y.; Ongsomwang, S. Land Use and Land Cover Scenarios for Optimum Water Yield and Sediment Retention Ecosystem Services in Klong U-Tapao Watershed, Songkhla, Thailand. *Sustainability* **2019**, *11*, 2895. [[CrossRef](#)]
15. Scott, D.A. *A Directory of Asian Wetlands*; IUCN Publication: Slimbridge Gloucester, UK, 1989; p. 1488.
16. Rattanadaeng, P.; Panboon, K.; Soe-been, S. *Structure and Distribution of Fish Community in Kwan Phayao, Phayao Province*; 53–0577–53033-002; Sukhothai Inland Fisheries Research and Development Center, Inland Fisheries Research and Development Division, Department of Fisheries, Ministry of Agriculture and Cooperatives: Bangkok, Thailand, 2015; pp. 1–95.
17. Kaewsri, K.; Traichaiyaporn, S. Monitoring on water quality and algae diversity of Kwan Phayao, Phayao Province, Thailand. *J. Agric. Technol.* **2012**, *8*, 537–550.
18. Peerapornpisal, Y.; Suphan, S.; Ngearnpat, N.; Pekkoh, J. Distribution of chlorophytic phytoplankton in Northern Thailand. *Biologia* **2008**, *63*, 852–858. [[CrossRef](#)]
19. Department of Public Works and Town & Country Planning. *Eradication of Water Hyacinth and Aquatic Weeds's Report*; Town and Country Development Bureau: Bangkok, Thailand, 2010.
20. Royal Irrigation Department. *Natural Development Planning*; Royal Irrigation Department: Bangkok, Thailand, 2017.
21. Inland Fisheries Research and Development Regional Center 1 (Phayao) Department of Fisheries. *Kwan Phayao*; Department of Fisheries: Phayao, Thailand, 2020.
22. Land Development Department. *Agri-Map. Soil erosion in Thailand (In Thailand)*; Ministry of Agriculture and Cooperatives: Bangkok, Thailand, 2000.
23. Land Development Department. *Agri-Map. Bangkok, Thailand, Office of Land Use Policy and Plan*; Ministry of Agriculture and Cooperatives: Bangkok, Thailand, 2018.
24. NCAR GIS Program Climate System Model, USA, June 2004 Version 3.0. Available online: <http://www.gisclimatechange.org> (accessed on 1 January 2020).
25. Mekong River Commission. *Basin-Wide Assessments of Climate Change Impacts on Water and Water-related Resources and Sector in Lower Mekong Basin, Technical Report: Ecosystem Component, Sub-Component II: Basin-Wide Impacts of Climate Change on Ecosystem Services in the Lower Mekong Basin*; Version: 1st Draft; Mekong River Commission Planning Division, Mekong River Commission for Sustainable Development: Vientiane, Laos, 2017; pp. 1–99.
26. Verburg, P.H.; Overmars, K.P. Combining top-down and bottom-up dynamics in land use modeling: Exploring the future of abandoned farmlands in Europe with the Dyna-CLUE model. *Landsc. Ecol.* **2009**, *24*, 1167–1181. [[CrossRef](#)]
27. Leh, M.D.K.; Matlock, M.D.; Cummings, E.C.; Nalley, L.L. Quantifying and mapping multiple ecosystem services change in West Africa. *Agric. Ecosyst. Environ.* **2013**, *165*, 6–18. [[CrossRef](#)]
28. Rouse, J.W. *Monitoring the Vernal Advancement of Retrogradation (Green Wave Effect) of Natural Vegetation*; NASA/GSFC Type III. Final. Rep; NASA: Greenbelt, MD, USA, 1974.
29. Hardisky, M.; Klemas, V.; Smart, A. The influence of soil salinity, growth form, and leaf moisture on the spectral radiance of *Spartina Alterniflora* canopies. *Photogramm. Eng. Remote Sens.* **1983**, *48*, 77–84.
30. Huete, A. A soil-adjusted vegetation index (SAVI). *Remote Sens. Environ.* **1988**, *25*, 295–309. [[CrossRef](#)]
31. Xu, H. Modification of Normalized Difference Water Index (NDWI) to Enhance Open Water Features in Remotely Sensed Imagery. *Int. J. Remote Sens.* **2006**, *27*, 3025–3033. [[CrossRef](#)]
32. Van der Linden, S.; Rabe, A.; Held, M.; Jakimow, B.; Leitão, P.J.; Okujeni, A.; Schwieder, M.; Suess, S.; Hostert, P. The EnMAP-Box—A Toolbox and Application Programming Interface for EnMAP Data Processing. *Remote Sens.* **2015**, *7*, 11249–11266. [[CrossRef](#)]
33. Congalton, R.; Green, K. *Assessing the Accuracy of Remotely Sensed Data: Principles and Practices*, 3rd ed.; CRC Press: Boca Raton, FL, USA, 30 September 2020.
34. Coppin, P.; Jonckheere, I.; Nackaerts, K.; Muys, B.; Lambin, E. Review Article Digital Change Detection Methods in Ecosystem Monitoring: A review. *Int. J. Remote Sens.* **2004**, *25*, 1565–1596. [[CrossRef](#)]
35. Jensen, J.R. *Introductory Digital Image Processing: A Remote Sensing Perspective*; Prentice-Hall Press: Hoboken, NJ, USA, 2015.
36. Mamat, A.; Halik, Ü.; Rouzi, A. Variations of Ecosystem Service Value in Response to Land-Use Change in the Kashgar Region, Northwest China. *Sustainability* **2018**, *10*, 200. [[CrossRef](#)]
37. Iamchuen, N.; Thep Wong, W. Relationship between Physical Factors and Land Use for the Future Land Use Prediction. *J. Archit./Plan. Res. Stud.* **2020**, *17*, 79–92.
38. Traore, A.; Watanabe, T. Modeling Determinants of Urban Growth in Conakry, Guinea: A Spatial Logistic Approach. *Urban Sci.* **2017**, *1*, 12. [[CrossRef](#)]

39. Kamwi, J.M.; Cho, M.A.; Kaetsch, C.; Manda, S.O.; Graz, F.P.; Chirwa, P.W. Assessing the Spatial Drivers of Land Use and Land Cover Change in the Protected and Communal Areas of the Zambezi Region, Namibia. *Land* **2018**, *7*, 131. [[CrossRef](#)]
40. Verburg, P.H.; Lesschen, J.P. *Practical: Explorative Modeling of Future Land Use for the Randstad Region of the Netherlands*; Wageningen University: Wageningen, The Netherlands, 2014.
41. Verburg, P.H.; Soepboer, W.; Veldkamp, A.; Limpiada, R.; Espaldon, V.; Mastura, S.S.A. Modeling the Spatial Dynamics of Regional Land Use: The CLUE-S Model. *Environ. Manag.* **2002**, *30*, 391–405. [[CrossRef](#)]
42. Ongsomwang, S.; Iamchuen, N. Integration of geospatial models for optimum land use allocation in three different scenarios. *Suranaree J. Sci. Technol.* **2015**, *22*, 19.
43. Renard, K.G.; Freimund, J.R. Using monthly precipitation data to estimate the R-factor in the revised USLE. *J. Hydrol.* **1994**, *157*, 287–306. [[CrossRef](#)]
44. Wischmeier, W.H.; Smith, D.D. *Predicting Rainfall Erosion Losses. A Guide to Conservation Planning*; The USDA Agricultural Handbook No. 537; USDA: Maryland, MD, USA, 1978.
45. Desmet, P.J.J.; Govers, G. A GIS procedure for automatically calculating the USLE LS factor on topographically complex landscape units. *J. Soil Water Conserv.* **1996**, *51*, 427–433.
46. Borselli, L.; Cassi, P.; Torri, D. Prolegomena to sediment and flow connectivity in the landscape: A GIS and field numerical assessment. *CATENA* **2008**, *75*, 268–277. [[CrossRef](#)]
47. Vigiak, O.; Borselli, L.; Newham, L.T.H.; McInnes, J.; Roberts, A.M. Comparison of conceptual landscape metrics to define hillslope-scale sediment delivery ratio. *Geomorphology* **2012**, *138*, 74–88. [[CrossRef](#)]
48. Sharp, R.; Douglass, J.; Wolny, S.; Arkema, K.; Bernhardt, J.; Bierbower, W.; Chaumont, N.; Denu, D.; Fisher, D.; Glowinski, K.; et al. *InVEST 3.8.9.post0+ug.gc993a4f.d20201118 User's Guide*; The Natural Capital Project; Stanford University, University of Minnesota, The Nature Conservancy, and World Wildlife Fund: Stanford, CA, USA, 2020.
49. Mayer, P.M.; Reynolds, K.R., Jr.; McCutchen, M.D.; Canfield, T.J. Meta-Analysis of Nitrogen Removal in Riparian Buffers. *J. Environ. Qual.* **2007**, *36*, 1172–1180. [[CrossRef](#)]
50. Zhang, X.; Liu, X.; Zhang, M.; Dahlgren, R.A.; Eitzel, M. A review of vegetated buffers and a meta-analysis of their mitigation efficacy in reducing nonpoint source pollution. *J. Environ. Qual.* **2010**, *39*, 76–84. [[CrossRef](#)]
51. Moriasi, D.; Arnold, J.; Liew, M.; Bingner, R.; Harmel, R.D.; Veith, T. Model Evaluation Guidelines for Systematic Quantification of Accuracy in Watershed Simulations. *Trans. ASABE* **2007**, *50*, 885–900. [[CrossRef](#)]
52. Me, W.; Abell, J.M.; Hamilton, D.P. Effects of hydrologic conditions on SWAT model performance and parameter sensitivity for a small, mixed land use catchment in New Zealand. *Hydrol. Earth Syst. Sci.* **2015**, *19*, 4127–4147. [[CrossRef](#)]
53. Xu, L.; Li, Z.; Song, H.; Yin, H. Land-Use Planning for Urban Sprawl Based on the CLUE-S Model: A Case Study of Guangzhou, China. *Entropy* **2013**, *15*, 3490–3506. [[CrossRef](#)]
54. Zhang, L.; Zhang, S.; Huang, Y.; Cao, M.; Huang, Y.; Zhang, H. Exploring an Ecologically Sustainable Scheme for Landscape Restoration of Abandoned Mine Land: Scenario-Based Simulation Integrated Linear Programming and CLUE-S Model. *Int. J. Environ. Res. Public Health* **2016**, *13*, 354. [[CrossRef](#)]
55. Bouguerra, S.; Jebari, S.; Tarhouni, J. An analysis of sediment production and control in Rmel river basin using InVEST Sediment Retention model. *J. New Sci. Agric. Biotechnol.* **2019**, *66*, 4170–4181.
56. Hamel, P.; Chaplin-Kramer, R.; Sim, S.; Mueller, C. A new approach to modeling the sediment retention service (InVEST 3.0): Case study of the Cape Fear catchment, North Carolina, USA. *Sci. Total Environ.* **2015**, *524–525*, 166–177. [[CrossRef](#)] [[PubMed](#)]
57. Sánchez-Canales, M.; López-Benito, A.; Acuña, V.; Ziv, G.; Hamel, P.; Chaplin-Kramer, R.; Elorza, F.J. Sensitivity analysis of a sediment dynamics model applied in a Mediterranean river basin: Global change and management implications. *Sci. Total Environ.* **2015**, *502*, 602–610. [[CrossRef](#)] [[PubMed](#)]
58. Perović, V.; Kadović, R.; Djurdjević, V.; Braunović, S.; Čakmak, D.; Mitrović, M.; Pavlović, P. Effects of changes in climate and land use on soil erosion: A case study of the Vranjska Valley, Serbia. *Reg. Environ. Chang.* **2019**, *19*, 1035–1046. [[CrossRef](#)]
59. Aneseyee, A.B.; Elias, E.; Soromessa, T.; Feyisa, G.L. Land use/land cover change effect on soil erosion and sediment delivery in the Winike watershed, Omo Gibe Basin, Ethiopia. *Sci. Total Environ.* **2020**, *728*, 138776. [[CrossRef](#)]
60. Han, H.; Yang, J.; Ma, G.; Liu, Y.; Zhang, L.; Chen, S.; Ma, S. Effects of land-use and climate change on sediment and nutrient retention in Guizhou, China. *Ecosyst. Health Sustain.* **2020**, *6*, 1810592. [[CrossRef](#)]
61. Redhead, J.W.; May, L.; Oliver, T.H.; Hamel, P.; Sharp, R.; Bullock, J.M. National scale evaluation of the InVEST nutrient retention model in the United Kingdom. *Sci. Total Environ.* **2018**, *610–611*, 666–677. [[CrossRef](#)]
62. Benez-Secanho, F.J.; Dwivedi, P. Does Quantification of Ecosystem Services Depend Upon Scale (Resolution and Extent)? A Case Study Using the InVEST Nutrient Delivery Ratio Model in Georgia, United States. *Environments* **2019**, *6*, 52. [[CrossRef](#)]
63. Yan, Y.; Guan, Q.; Wang, M.; Su, X.; Wu, G.; Chiang, P.; Cao, W. Assessment of nitrogen reduction by constructed wetland based on InVEST: A case study of the Jiulong River Watershed, China. *Mar. Pollut. Bull.* **2018**, *133*, 349–356. [[CrossRef](#)]
64. Singh, N.K.; Gourevitch, J.D.; Wemple, B.C.; Watson, K.B.; Rizzo, D.M.; Polasky, S.; Ricketts, T.H. Optimizing wetland restoration to improve water quality at a regional scale. *Environ. Res. Lett.* **2019**, *14*, 064006. [[CrossRef](#)]
65. Mei, Y.; Kong, X.; Ke, X.; Yang, B. The Impact of Cropland Balance Policy on Ecosystem Service of Water Purification—A Case Study of Wuhan, China. *Water* **2017**, *9*, 620. [[CrossRef](#)]
66. Rosenfield, G.H.; Fitzpatrick-Lins, K. A coefficient of agreement as a measure of thematic classification accuracy. *Photogramm. Eng. Remote Sens.* **1986**, *52*, 223–227.

67. Anderson, J.R.; Hardy, E.E.; Roach, J.T.; Witmer, R.E. *A Land Use and Land Cover Classification System for Use with Remote Sensor Data*; US Government Printing Office: Washington, DC, USA, 1976; Volume 964.
68. Al-doski, J.; Mansor, S.B.; Shafri, H.Z.M. Support vector machine classification to detect land cover changes in Halabja City, Iraq. In Proceedings of the 2013 IEEE Business Engineering and Industrial Applications Colloquium (BEIAC), Langkawi, Malaysia, 7–9 April 2013; pp. 353–358.
69. Taati, A.; Sarmadian, F.; Mousavi, A.; Pour, C.T.H.; Shahir, A.H.E. Land Use Classification using Support Vector Machine and Maximum Likelihood Algorithms by Landsat 5 TM Images. *Walailak J. Sci. Technol.* **2015**, *12*, 681–687.
70. Bouaziz, M.; Eisold, S.; Guermazi, E. Semiautomatic approach for land cover classification: A remote sensing study for arid climate in southeastern Tunisia. *Euro-Mediterr. J. Environ. Integr.* **2017**, *2*, 24. [[CrossRef](#)]
71. Mandal, S.; Saha, A. Support vector machines for monitoring land use dynamicity and temporal variation of land surface temperature in Kurseong and surrounding of Darjeeling Himalaya. *Model. Earth Syst. Environ.* **2018**, *4*, 659–672. [[CrossRef](#)]
72. Foody, G.; Mathur, A. The use of small training sets containing mixed pixels for accurate hard image classification: Training on mixed spectral responses for classification by a SVM. *Remote Sens. Environ.* **2006**, *103*, 179–189. [[CrossRef](#)]
73. Chen, H.; Zhang, W.; Gao, H.; Nie, N. Climate Change and Anthropogenic Impacts on Wetland and Agriculture in the Songnen and Sanjiang Plain, Northeast China. *Remote Sens.* **2018**, *10*, 356. [[CrossRef](#)]
74. Degife, A.; Worku, H.; Gizaw, S. Environmental implications of soil erosion and sediment yield in Lake Hawassa watershed, south-central Ethiopia. *Environ. Syst. Res.* **2021**, *10*, 28. [[CrossRef](#)]
75. Zhou, M.; Deng, J.; Lin, Y.; Belete, M.; Wang, K.; Comber, A.; Huang, L.; Gan, M. Identifying the effects of land use change on sediment export: Integrating sediment source and sediment delivery in the Qiantang River Basin, China. *Sci. Total Environ.* **2019**, *686*, 38–49. [[CrossRef](#)]
76. Yang, X.; Ji, G.; Wang, C.; Zuo, J.; Yang, H.; Xu, J.; Chen, R. Modeling nitrogen and phosphorus export with InVEST model in Bosten Lake basin of Northwest China. *PLoS ONE* **2019**, *14*, e0220299. [[CrossRef](#)]
77. Han, B.; Reidy, A.; Li, A. Modeling nutrient release with compiled data in a typical Midwest watershed. *Ecol. Indic.* **2021**, *121*, 107213. [[CrossRef](#)]
78. Raji, S.A.; Odunuga, S.; Fasona, M. Spatiotemporal Modeling of Nutrient Retention in a Tropical Semi-Arid Basin. *Environ. Res. Technol.* **2020**, *3*, 225–237.